# **Exploring Internal Magnetism in Partially Suppressed Red Giant Stars**

by

#### Kanah Marie Smith

October, 2025

A thesis submitted to the
Graduate School
of the
Institute of Science and Technology Austria
in partial fulfillment of the requirements
for the degree of
Master of Science

Committee in charge:

Lisa Bugnet, Supervisor
Paul Beck
Ylva Götberg
Caroline Muller



The thesis of Kanah Marie Smith, titled <i>Exploring Internal Magnetism in Pa</i> Red Giant Stars, is approved by:	rtially	Suppressed
Supervisor: Lisa Bugnet, ISTA, Klosterneuburg, Austria		
Signature:		
Committee Member: Paul Beck, Universidad de La Laguna & Instituto Canarias La Laguna, Santa Cruz de Tenerife, Spain	de Ast	crofisica de
Signature:		
Committee Member: Ylva Götberg, ISTA, Klosterneuburg, Austria		
Signature:		
Committee Member: Caroline Muller, ISTA, Klosterneuburg, Austria		
Signature:		

#### © by Kanah Marie Smith, October, 2025 All Rights Reserved

ISTA Master's Thesis, ISSN: 2791-4585

I hereby declare that this thesis is my own work and that it does not contain other people's work without this being so stated; this thesis does not contain my previous work without this being stated, and the bibliography contains all the literature that I used in writing the dissertation.

I accept full responsibility for the content and factual accuracy of this work, including the data and their analysis and presentation, and the text and citation of other work.

I declare that this is a true copy of my thesis, including any final revisions, as approved by my thesis committee, and that this thesis has not been submitted for a higher degree to any other university or institution.

I certify that any republication of materials presented in this thesis has been approved by the relevant publishers and co-authors.

Signature: \_\_\_\_\_

Kanah Marie Smith October, 2025

#### **Abstract**

The internal dynamical properties of red giant stars have been explored extensively in recent years as a result of the increase in high precision data availability from the space missions Kepler and TESS (Transiting Exoplanet Survey Satellite), and in this exploration, it has been discovered that some of these stars are not behaving as expected. Red giants are stars that have evolved off of the main sequence after having completed fusing hydrogen into helium in their core. Observational data shows that the cores are rotating significantly slower than models can recreate consistently across evolutionary stages. This discrepancy has prompted investigation into the efficiency of angular momentum transport mechanisms and mixing processes including meridional circulation, shear instability, internal gravity waves, Tayler-Spruit dynamo, fossil magnetic fields etc., to explain this behavior.

Analyzing seismic oscillations in stars, via asteroseismology, is a powerful tool as it is the only way in which the deep stellar interior can be probed and subsequently characterized; this is possible as global oscillations modulating the stellar surface are effected by internal processes. For red giants, p-modes (pressure modes; resonating through the entire star) and g-modes (gravity-modes; resonating in the radiative interior) couple to create mixed modes. These mixed modes give access to the otherwise hidden stellar interior as g-modes couple to p-modes, delivering information from the interior to the surface.

Internal magnetic signatures have been observationally confirmed in red giant stars via asteroseismology and characterized in two ways. One being that dipole mixed modes with  $\ell=1$  will display a global asymmetric frequency shift of its azimuthal components; where the m=0 and  $m=\pm 1$  components of the  $\ell=1$  dipole mode will be shifted by two different power laws, respectively. And the other being a reduced visibility of dipole mixed mode amplitudes in the power spectra, where stars presenting with this feature are denoted as suppressed.

Several studies of the suppressed dipole mixed mode amplitudes have been carried out, but thus far, no dedicated studies of the asymmetric frequency shifts of suppressed red giants have been conducted; one reason being that the asymmetric frequency shifts cannot be characterized when the dipole mixed mode amplitudes are severely reduced in many of the suppressed stars.

Since fully suppressed stars do not have detectable mixed-modes to evaluate, partially suppressed stars, that is, red giant stars presenting with suppressed dipole mixed modes in *select parts* of their power spectra rather than across the entire spectra, will be the subject of this study as the respective mode amplitudes are still visible at high frequencies.

As such, this study will search for asymmetric frequency shifts on the dipole mixed modes of partially suppressed red giant stars; the aim here is to investigate if both mode suppression and magnetic shifting of dipole mixed modes occur simultaneously.

This study will be conducted by creating a pipeline to estimate priors of asteroseismic parameters, use the priors to model the power spectra with the stellar modeling code *sloscillations\_ISTA*,

and perform a Bayesian fit of the parameters with the simulated data on the star KIC 6975038, a target with partially suppressed dipolar mode amplitudes identified in the literature, to fit its magnetic parameters. I present a novel method to model the stellar power spectra of partially suppressed red giants by application of a sigmoid profile to the  $\ell=1$  dipolar mode component of the spectra. With the results of this study I aim at constraining the cause of this partial dipole mode amplitude suppression, allowing for more detailed studies regarding their astrophysical nature. Furthermore, the long term hope for the method used in this study will be to expand the sample of partially suppressed red giants and fit their asteroseismic parameters accordingly.

## Acknowledgements

This paper includes data collected by the Kepler mission and obtained from the MAST data archive at the Space Telescope Science Institute (STScI). Funding for the Kepler mission is provided by the NASA Science Mission Directorate. STScI is operated by the Association of Universities for Research in Astronomy, Inc., under NASA contract NAS 5–26555.

#### **About the Author**

Kanah Marie Smith completed an Honors Bachelor of Science (HBSc) at the University of Toronto with a major in Astronomy & Astrophysics; minors in French Language, and Environment & Energy; with a certificate in Sustainable Pathways before joining ISTA in September of 2023. Her main research interests include creating ensemble pipelines for the analysis of large stellar physics data sets.

# **Table of Contents**

Αŀ	bstract	vii
Αc	cknowledgements	ix
Αŀ	bout the Author	x
Ta	able of Contents	xi
Lis	st of Figures	xi
Lis	st of Tables	xiv
1	Introduction	1
2	Data Preparation         2.1 Photometric Data          2.2 Background and Power Excess          2.3 Fitting the Background and Power Excess with apollinaire          2.4 Dipole Mode Visibility	<b>5</b> 5 5 6 7
3	Methods3.1 PSD Modeling & Additional Relevant Parameters	<b>15</b> 15 19
4	Results         4.1       KIC 8684542: A "Normal" Red Giant          4.2       KIC 6975038          4.2.1       Sigmoid Profile of a Partially Suppressed Red Giant          4.2.2       KIC 6975038: The Unusual Red Giant	21 21 22 22 24
5	Discussion, Conclusions, & Interpretations	29
Bi	ibliography	31

# **List of Figures**

1.1	Octupole $\ell=3$ oscillation modes are illustrated here at a frozen moment in time, at different stellar orientations to the observer. The columns show the stellar surface inclined at $30^\circ$ on the left, $60^\circ$ in the center, and $90^\circ$ on the right. While the rows depict the orientations of the white surface nodes for the azimuthal order $m$ such that $m \in [-3,3]$ . As $m$ defines the number of surface nodes oriented longitudinally, the top row shows $m=0$ where all surface nodes are lines of latitude, the second row shows $m=\pm 1$ with one line of longitude, the third row shows $m=\pm 2$ with two lines of longitude, and the fourth row shows $m=\pm 3$ wherein all surface nodes are longitudinal. Additionally, the blue and red regions display the opposing compression and expansion of the region. This figure is a modification of figure 1.4 in [ACK10, sec 1 pg 14]	2
2.1	The background fit for the PSD of KIC 6975038, using apollinaire [BGB $^+$ 22], shows the original data in black and grey; the boundary of the two illustrates the default low frequency cut-off of $10\mu{\rm Hz}$ in which around this point the active region dominates the spectrum at lower frequencies. The effects can be seen with the upwards sloping of the spectrum below this point. The initial guess and fitted background are shown in blue and red respectively, with the the components matching in color with dotted and dashed lines. The constant white noise from the instrument is also shown in cyan and visible is the spectrum at high frequencies when all other components approach zero	7
2.2	Extracted from [SCF+16a] figure 4, the dipole mode visibilities $V_{\ell=1}^2$ for 3611 Kepler red giants are plotted against their frequency at maximum power $\nu_{max}$ . The colors indicate the stellar mass in solar mass units $M_{\odot}$ , and are scaled following the color bar on the right of the figure. The dotted line is adopted from [SCF+16b] and separates the stars with normal stars from those showing suppressed dipole mode amplitudes. The black lines are showing the estimated visibilities from stellar models for a range of stellar masses (1.1, 1.3, 1.5, 1.7, 1.9 [ $M_{\odot}$ ]) wherein the average lifetime of a mode is 20 days following the peakbagging analysis of [CDG15] section 2. The gray lines are similarly showing the estimated visibilities from a $1.7M_{\odot}$ stellar model, but with the average mode lifetime just 10 days, and an average mode lifetime just under 40 days. The depiction of varying mode lifetimes shows the slight dependence of $V_{\ell=1}^2$ on these lifetimes with the gray lines being distinct, while highlighting the lack of dependence on the stellar mass for the black lines which mostly overlap one another	9
2.3	PSD of the sample star KIC 8684542 showing the original data in black segmented into the regions of $\ell=0,1,2,3$ , following the masking formalism of [SCF+16a, SCF+16b] shown in equation 2.4. The colors are attributed to the oscillation modes as follows: $\ell=0$ is blue, $\ell=1$ is red, $\ell=2$ is green, and $\ell=3$ is yellow. In this work, KIC 8684542 is representative of a "normal" red giant presenting with dipole mixed modes. The mixed mode characteristic where the power density of a single $\ell=1$ mode being redistributed within this region is visible in comparison to	
	the mostly singular peaks of $\ell = 0, 2, 3, \ldots$	10

2.4	PSD of the sample star KIC 2018283, with the same segmentation of mode frequency regions as in figure 2.3. Of note for this star is the suppression of the dipole mixed mode $\ell=1$ in the red regions; shown in [SCF <sup>+</sup> 16b] figure 1. In this work, KIC 2018283 will serve as the fully suppressed star example	10
2.5	PSD of the sample star KIC 6975038, with the same segmentation of mode frequency regions as in figures 2.3 and 2.4. The notable feature that makes this target the main star of this work is the partially suppressed dipole mode amplitudes seen in the red $\ell=1$ regions. Noted for the unusual partial suppression in [MBP+17], [MPB+17], [Loi20], [DLBL23], [ROM23], and [AT24] this star was reported by [DLBL23] to have a magnetic field strength around 180 kilo-Gauss in the hydrogen burning shell surrounding the core. The suppression of low frequency dipole $\ell=1$ mixed modes is attributed to the field, although the appearance of high frequency $\ell=1$ modes requires further investigation of magnetic signatures on this star, namely frequency shifts	11
2.6	Dipole mode visibilities $V_{\ell=1}^2$ calculated in this study using the oscillation mode regions in 2.4. KIC 6975038, KIC 8684542, and KIC 2018283 are highlighted as star points in bright pink, orange, and green respectively. KIC 8684542 resides in the "normal" region of visibility around 1.35 [SCF+16a] with $V_{\ell=1}^2\approx 1.30$ . KIC 2018283 resides in the suppressed mode region, around 0.5 or down to zero for the least evolved stars, with $V_{\ell=1}^2\approx 0.21$ . KIC 6975038 resides in the intermediate region between the two previous stars, as we expect for a star with only partially suppressed mode amplitudes, with $V_{\ell=1}^2\approx 0.45$ .	12
2.7	Dipole mode visibilities $V_{\ell=1}^2$ calculated in this study using the oscillation mode regions in 2.4; differently from figure 2.6, here the Gaussian weighted average of figure 2.2 has been multiplied to each star. The positions relative to one another remain the same for the highlighted stars KIC 6975038, KIC 8684542, and KIC 2018283, shown as star points in bright pink, orange, and green respectively. KIC 8684542 resides on the "normal" branch of visibility with $V_{\ell=1}^2 \approx 0.47$ . KIC 2018283 resides in the suppressed mode region with $V_{\ell=1}^2 \approx 0.05$ . KIC 6975038 resides in the intermediate region between the two previous stars with $V_{\ell=1}^2 \approx 0.13$ .	13
3.1	Symmetric splitting of the dipole mixed mode frequencies into the azimuthal components $m=0,\pm 1$ following equations 3.7 and 3.9. The top panel of the figure shows the dipole mixed mode without rotational perturbation, while the bottom illustrates the splitting of the modes in the rotating case showing that $m=0$ remains stationary while $m=\pm 1$ will shift in equal and opposite directions.	17
3.2	Asymmetric magnetic splitting of the dipole mixed mode frequency azimuthal components $m=0,\pm 1$ following equation 3.10. The top panel is identical to that in figure 3.1 showing the dipole mixed mode, in this case without magnetic perturbation, while the bottom panel illustrates the splitting of the mode caused by magnetic perturbation. It can be seen here that the $m=0$ component of the mode shifts to higher frequencies by half as much as the $m=\pm 1$ components which shift by the same amount.	18
4.1	The resultant PSD of KIC 8684542 is shown in red plotted over the original data in black. For ease in locating the $\ell=1$ dipole mode regions, the $\ell=0,2,3$ modes are highlighted with star markers in the colors purple, pink, and blue respectively, such that the $\ell=1$ oscillation modes reside between the $\ell=2$ and $\ell=3$ modes.	22
	such that the $t-1$ oscination modes reside between the $\ell=2$ and $\ell=3$ modes.	

4.2	The Sigmoid function plotted with the red dashed line is created using equation 4.1 for the relevant frequency range of the partially suppressed star KIC 6975038. The vertical blue line shows $\nu_{max}\approx 125.24~[\mu {\rm Hz}]$ , and the blue star shows the inflection or mid-point (50% mode suppression) of the Sigmoid function with a default setting at $\nu_{max}$ . The Sigmoid function has a sharp change of behaviour	
	from 0% to 100% to imitate the change from total suppression to the reappearance of the dipole $\ell=1$ mixed mode; with this transition occurring near $\nu_{max}$ , justifying	
	the choice to set the inflection point at $\nu_{max}$	24
4.3	The resultant PSD of KIC 6975038 is shown in red plotted over the original data in black. In addition to what is shown in figure 4.1, the sigmoid profile used to modulate the dipolar component of the spectrum is illustrated by the orange dashed curve. For clarity in locating the $\ell=1$ dipole mode regions, the $\ell=0,2,3$ modes are highlighted with purple, pink, and blue stars respectively, such that the	
4.4	$\ell=1$ oscillation modes reside between the $\ell=2$ and $\ell=3$ modes The posterior distribution of the <code>Bayessloscillations_ISTA</code> (Desai et al. in prep.) fit for the power spectrum of KIC 6975038 is shown, illustrating that some of the parameters, namely $\theta_{inc}, \epsilon_g$ and $\delta\nu_{mag}$ , are not as well constrained as $q, \Delta\nu$ or $\epsilon_p$ . Of note is the distribution for $\Delta\Pi_{\ell=1}$ , which is in agreement with red giant values ( $\sim 50 < \Delta\Pi_{\ell=1} < \sim 150$ ) according to [MBB+14], although the value is on the	25
4.5	lower end of this boundary and so further evaluation of this behavior is needed. The MCMC walker chains of the <i>Bayessloscillations_ISTA</i> (Desai et al. in prep.) fit for the power spectrum of KIC 6975038 is shown and illustrates the parameter	26
	exploration of the walkers	27

## **List of Tables**

3.1	List of the model parameters involved in the Bayesian fitting in Bayessloscillations_ISTA (Desai et al. in prep.). All parameters except for $\Delta\nu$ are sampled from a uniform distribution bounded by the ranges given in column 2. $\Delta\nu$ is sampled from a Gaussian distribution with a standard deviation $\sigma=0.15$ ; the reason for this narrow sampling range is to because the $\Delta\nu$ values for Kepler red giants are well studied and well constrained, so the parameter space exploration does not need to be large.	19
4.1	List of the fit model parameters from <i>Bayessloscillations_ISTA</i> (Desai et al. in prep.) for KIC 8684542 including the respective errors measured as the difference between the mean and 16th and 84th percentiles from the resultant MCMC chain of walkers.	23
4.2	List of the fit model parameters from <i>Bayessloscillations_ISTA</i> (Desai et al. in prep.) including the respective errors measured as the difference between the mean and 16th and 84th percentiles from the resultant MCMC chain of walkers.	25

CHAPTER 1

#### Introduction

Our Sun is currently in its longest evolutionary stage as a main sequence star, producing energy through nuclear fusion by burning hydrogen into helium. And despite being our nearest star, there is still much we do not know about its internal processes including rotation rate, chemical mixing, density profiles etc. In contrast, surface processes like solar wind and heating mechanisms of the corona have been well studied [DFP95]. The near surface solar magnetic field has been characterized via photometry (measuring changes to visible light), in addition to spectroscopy (changes to characteristic emission and absorption of light) and spectropolarimetry (measuring the polarization rate of light) (see eg., [EHI+94, GGC+95, HHH+96, FAA+97, GAC+08]), which are used to measure surface magnetic activity in other stars as well.

In this work I aim to understand core magnetic fields. Stellar magnetism is widely known to play an important part in stars across the evolutionary spectrum, notably in the transport of angular momentum, which has significant impacts on stellar lifetimes via mixing. But spectroscopy and spectropolarimetry remain blind to direct observations of internal magnetic fields. The only way to explore the deep stellar interior is by studying stellar seismic waves via asteroseismology. Modern day high-precision photometry of red giants from space missions including CoRoT (CNES; [MBA+06]), Kepler (NASA; [BKB+10]), and TESS (NASA; [RWV+14]) have provided the spark to investigate internal magnetism in these stars as evaluations of this data showed that the interiors of red giants are rotating slower than theory at the time had predicted [SP00, MGB+12a]; meaning that angular momentum redistribution was being facilitated by more than just hydrodynamical processes (those processes including the turbulent movement of material and consequential transfer of angular momentum). This finding motivated theories wherein an internal magnetic field originates from dynamo action at the radiative zone (see eg., [CMB+14]), or as a remnant field from the progenitor (see eg., [CFB16, FPJ19, BPM+21]), denoted as a fossil field. Although, a conclusion on the origins of this internal magnetic field has not yet been reached, and the search continues.

The work presented in this study is motivated by the hope to constrain the origin(s) of this internal field by obtaining a better understanding of its behaviour. I will be investigating red giant stars presenting with unique features in their stellar power spectra that are potentially the result of an internal magnetic field, doing so with asteroseismology as the key tool.

The study of seismic waves propagating through stars via asteroseismology provides the only

way to explore the deep stellar interior and evaluate stellar oscillation modes. Gravity waves (g-modes) are primarily induced by tangential perturbations of material and propagate through the stellar interior; while pressure/acoustic waves (p-modes) that are primarily induced by radial perturbations and propagate through the entire star, are more sensitive to the outer stellar regions. In seismology, we work to characterize the nature of these oscillations, and to do so we analyze the behaviour of particular modes. Each oscillation mode can be described by three quantum numbers/parameters  $\ell, m$ , and n, where  $\ell$  is the degree of the mode, stating the number of surface nodes of the wave; m is the azimuthal order of the mode, where |m| defines the number of surface nodes that are oriented in the longitudinal direction (while the rest are lines of latitude) and follows that  $m \in [-\ell, +\ell]$ ; and finally n is the overtone of the mode defining the radial node number of a particular mode [ACK10, chap. 1.3]. Configurations of  $\ell, m$ , and n on a sphere can be seen in figure 1.1, which shows the opposing pulsation of the body in red and blue, separated by white lines illustrating the surface nodes.

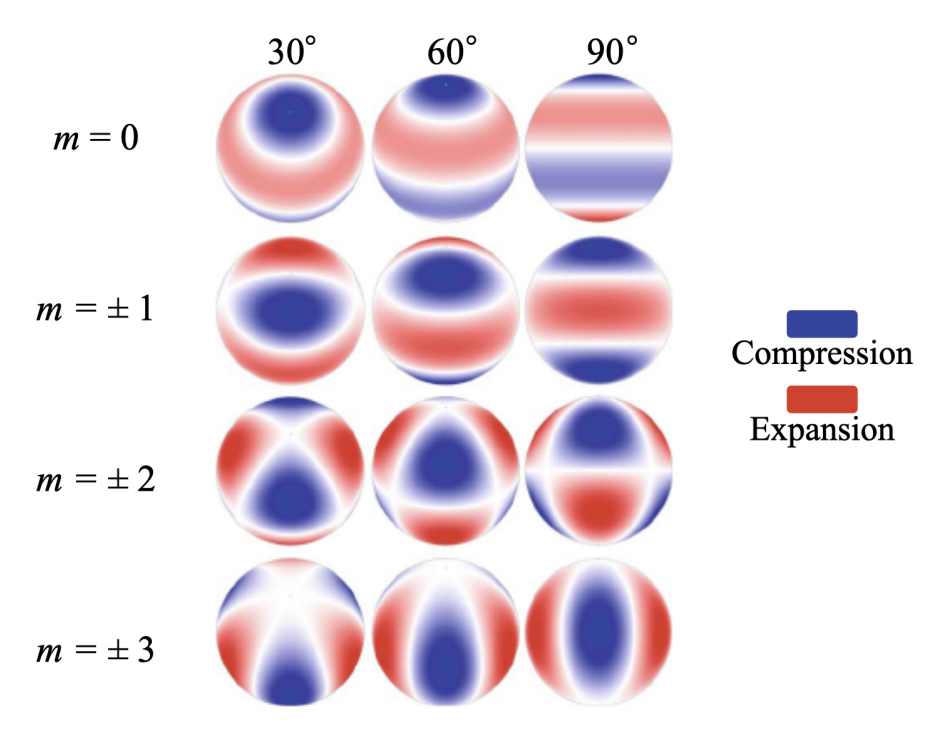


Figure 1.1: Octupole  $\ell=3$  oscillation modes are illustrated here at a frozen moment in time, at different stellar orientations to the observer. The columns show the stellar surface inclined at  $30^\circ$  on the left,  $60^\circ$  in the center, and  $90^\circ$  on the right. While the rows depict the orientations of the white surface nodes for the azimuthal order m such that  $m \in [-3,3]$ . As m defines the number of surface nodes oriented longitudinally, the top row shows m=0 where all surface nodes are lines of latitude, the second row shows  $m=\pm 1$  with one line of longitude, the third row shows  $m=\pm 2$  with two lines of longitude, and the fourth row shows  $m=\pm 3$  wherein all surface nodes are longitudinal. Additionally, the blue and red regions display the opposing compression and expansion of the region. This figure is a modification of figure 1.4 in [ACK10, sec 1 pg 14].

Subsequent acoustic oscillation modes with the same degree  $\ell=0$  will be evenly spaced in frequency by the term  $\Delta\nu$ , and the amplitude of oscillation will peak around the frequency  $\nu_{max}$ . Both of these terms,  $\Delta\nu$  and  $\nu_{max}$ , are characteristic to stellar evolutionary stages and are fundamental asteroseismic parameters for constraining core rotation rates (eg., [MEH+12, BDA+12, MVB+15, GMM+18, LDB24]), and stellar processes like the ignition of helium (or not) in the stellar core (eg., [BMH+11, CSH+12, VMS16, HSY17, HSY18]).

As the stellar interior is the location of this otherwise inaccessible information, access to it via seismology provides the only way to take a "peak" inside of a star. Seismic studies of the Sun with helio-seismology has allowed for the characterization of the outer convective regions via pressure modes (see eg., [DFP95]), but solar g-modes cannot be detected (see eg., [BPB22] for a detailed review on the status of g-mode amplitudes and detections in the Sun from previous studies). And, even if g-modes were to exist in the Sun, having high mode inertia resonating in high density regions of the star, their mode lifetimes would be significantly longer than those of p-modes; meaning that to be observationally detected, the data would need to have a much longer time basis than the 4 years with Kepler to detect the low frequencies. Looking forwards at the successive evolutionary stage for the Sun, red giant stars arise when main sequence stars deplete their core hydrogen supply. And although pure g-modes have still not been detected in red giants, unlike main sequence stars, red giants have a probe that confirms their presence.

Mixed modes are p-modes with both p- and g-mode characteristics and they can occur in red giant stars when the pressure and gravity mode frequencies become sufficiently close enough for the g-modes to couple with p-modes. This coupling is most notable on the  $\ell=1$  dipole mode as the acoustic component of the mode resonates close enough to the g-mode propagation zone in comparison to the  $\ell=2$  quadrupole modes. It is important to note that the  $\ell=0$  radial modes are pure-pressure modes that do not interact with gravity modes to have mixed character. Theoretical descriptions of mixed modes can be found in [DGHS01] and [Chr04] for example, and were first reported in *Kepler* red giants by [BBM+11].

Mixed modes can be present in red giant stars due to their structure, and the solar structure is the reason why we do not detect mixed modes in the Sun as the propagation region for g-modes is too far away from the p-mode propagation region for them to couple before the g-modes rapidly decay in the evanescent zone between these regions. Red giants with detectable mixed modes, like KIC 8684542 in figure 2.3, are unique in this way and serve as a laboratory for understanding internal gravity waves and stellar processes through the information relayed by gravity modes. Additionally, as they are so close to main sequence stars from an evolutionary stand point, studies of mixed modes in red giants allows for better understanding of the current deep interior processes and structure of the Sun as well as insight on what is to come in its future.

In recent years, internal magnetic fields have been observationally confirmed in red giants via signatures detected on dipolar mixed modes, including suppressed mode amplitudes [GPB<sup>+</sup>14, SCF<sup>+</sup>16a, SCF<sup>+</sup>16b], and mode frequency shifts [LDBL22, DLBL23, LDL<sup>+</sup>23, HON<sup>+</sup>24]; theoretical exploration of these frequency shifts are explored by [GL20, MBP<sup>+</sup>21, BPM<sup>+</sup>21, Bug22, Loi21, MB23, BDB<sup>+</sup>24, DEB24].

The internal magnetism theory first presented by [FCS<sup>+</sup>15] states that the suppressed  $\ell=1$  dipole mode amplitudes are attributed to a magnetic greenhouse effect wherein mixed mode energy is scattered and trapped within the radiative (interior) region when magnetic tension exceeds the restoring force of the wave.

Most of the red giants identified to have suppressed dipolar mode amplitudes display this feature across their entire frequency range (see [SCF+16a, SCF+16b]) as in KIC 2018283 seen in figure 2.4. But there a select few stars that display partial suppression of their dipolar mode amplitudes [GPB+14, DLBL23], where only high frequency  $\ell=1$  modes are visible; as is the case for KIC 6975038 seen in figure 2.5.

#### 1. Introduction

These red giants with partially suppressed modes will be the subject of my study as I work to characterize the source of this suppression. With the state of seismology focusing on detections of internal magnetic fields, the following question arises: are the visible mixed modes in partially suppressed stars carrying the signature of internal magnetism in the frequency pattern? By modeling the power spectra with a novel method and conducting a Bayesian fit of the asteroseismic parameters, in this thesis I work to answer this question.

This thesis is outlined as follows: in section 2 the origins of the data used in this study are detailed along with how that data is processed for asteroseismic analysis, section 3 introduces the method of modeling red giant power spectra, in addition to the novel method of this study wherein the profile of a partially suppressed red giant is estimated with a sigmoid profile; section 4 presents the results of Bayesian fitting for a target with partially suppressed mixed modes as well as a "normal" red giant whose mixed modes are entirely present; interpretation of the presented results are discussed in section 5 where the significance of the findings are contextualized within the current state of seismic studies and concludes on the findings, proposing future work that can stem from this study.

### **Data Preparation**

#### 2.1 Photometric Data

The photometric data used to conduct this study is the 30 minute long-cadence data from the *Kepler* Space Telescope [BKB $^+$ 10], accessed through The Mikulski Archive for Space Telescopes (MAST) and optimized for use in asteroseismology following the prescription of [GHS $^+$ 11].

Photometric time series data is obtained by way of continuous observation of a target star. *Kepler* data was chosen for this study, as the 4-year long continuous time basis of the observations provides opportunity to probe lower frequency oscillations. Additionally, the cadence times (1 minute short cadence, and 30 minute long cadence), and sensitivity of the instruments in combination with the 4-year observations means that the data in frequency has a high signal-to-noise ratio (SNR) (compared to CoRoT or TESS data), allowing for the detection of lower amplitude oscillations. The ability to achieve a high SNR is a key factor in how the *Kepler* mission revolutionized the field of asteroseismology and propelled the community into an era rich with data, as the telescope had observed several millions of stars during its commission.

The photometric time series received from the instrument is converted into the frequency domain by use of the Lomb-Scargle periodogram [Lom76, Sca82], a Fourier-like transformation for unequally spaced data. The resultant periodogram is called the **power spectrum density** (PSD) and can be seen in figure 2.1 for *Kepler Input Catalogue* (KIC) star KIC 6975038; the PSD illustrates the density of power attributed to photometric variations of light over a range of frequencies. Along with the power excess signal from oscillations centered around the frequency of maximum power  $\nu_{max}$  with a Gaussian profile [MBA+08], the PSD also contains signals denoted as the background noise (the dashed and dotted lines in figure 2.1) which comprises of constant instrumental noise and photospheric granulation dominating the low frequency range. To assess the pattern of the oscillations accurately, we work to estimate this background to ultimately remove it.

#### 2.2 Background and Power Excess

To conduct background estimation, I use the asteroseismic peak-bagging (extraction of stellar oscillation mode parameters) software apollinaire [BGB<sup>+</sup>22] to fit the background components.

Photospheric granulation near the stellar surface is the result of turbulent plasma cells causing the surface to take on a granular-look. There are various scales of granulation that can be present at the same time, but the stellar granulation can be well estimated with just 2 scales modeled by Lorentzian functions of the form

$$P(\nu) \propto \frac{1}{1 + (\pi \nu \tau)^c},\tag{2.1}$$

where  $\tau$  is the timescale of decay for the sudden pulse that arises on the stellar surface, while c dictates the shape of the Lorentzian profile and therefore the speed of exponential decay of the power [KDH+14]. [BGB+22] encode c=4 when using two Harvey-profiles, representing a symmetrically growing and decaying pulse [KDH+14]. These Lorentzian functions are denoted as Harvey profiles after [Har85] analyzed and characterized the shape of the various scales of granulation of the background to follow high-power Lorentzian profiles.

The power excess oscillation signal is classically described by a Gaussian profile centered around  $\nu_{max}$  [MBA<sup>+</sup>08] and is of the form

$$P(\nu) = H_{\nu_{max}} \exp\left[\frac{(\nu - \nu_{max})^2}{W_{env}^2}\right], \qquad (2.2)$$

where  $H_{\nu_{max}}$  is the height at  $\nu_{max}$ , and  $W_{env}$  is the full width at half max (FWHM) of the Gaussian power excess envelope.

Finally, the instrumental noise used to model the photon white noise in *apollinaire* [BGB $^+$ 22] follows the prescription of [MGR $^+$ 10] who use a constant term W, that is taken to be the mean power surrounding a cut-off frequency. It is expected that the photon noise will outweigh the other background components in this region such that the value can be taken as the constant term for the entire spectrum.

# 2.3 Fitting the Background and Power Excess with apollinaire

To use apollinaire [BGB<sup>+</sup>22] to fit the background of KIC 6975038, the background parameters priors are first estimated using the function

create\_background\_guess\_arrays with the input parameters radius  $R_{\star}$ , mass  $M_{\star}$ , effective temperature T,  $\nu_{max}$  and  $\Delta\nu$ , taken from the catalogue of [YHB+18], in addition to the PSD and frequency array. Using the parameter priors, the code is used in this study to fit the background parameters by way of Monte Carlo Markov Chain (MCMC) sampling implemented with the *Python* package *emcee* [FHLG13]. The MCMC set-up for the fitting includes 64 walkers iterated over 4500 steps each with the first 500 iterations discarded as burn-in.

Additionally, the background fitting begins at the low frequency cut off of  $10\mu$ Hz; this is done to avoid the part of the spectra in which the stellar active region dominates the signal from near surface activity [Har85]. The PSD of KIC 6975038 is seen in figure 2.1 where the fitted background components and oscillation power excess are shown in red.

When the model reaches convergence, that is, when the background parameters converge to values best fitting the real spectra, a summation of the instrumental noise and Harvey-profiles

# KIC 6975038 | The control of the co

Figure 2.1: The background fit for the PSD of KIC 6975038, using apollinaire [BGB $^+$ 22], shows the original data in black and grey; the boundary of the two illustrates the default low frequency cut-off of  $10\mu$ Hz in which around this point the active region dominates the spectrum at lower frequencies. The effects can be seen with the upwards sloping of the spectrum below this point. The initial guess and fitted background are shown in blue and red respectively, with the the components matching in color with dotted and dashed lines. The constant white noise from the instrument is also shown in cyan and visible is the spectrum at high frequencies when all other components approach zero.

are subtracted from the spectrum. The Gaussian profile of the power excess is constructed from the fitted parameters and will be applied to the spectrum as a weighted average in section 2.4. The resultant spectrum, with the background components removed, is now ready for the mode amplitudes to be analyzed. Section 2.4 will discuss how partially suppressed red giant stars are differentiated from normal and suppressed stars using their dipolar mode amplitudes.

#### 2.4 Dipole Mode Visibility

As the focus of this study is to investigate the seismic properties of red giants with partially suppressed dipolar modes, for future work on expanding the sample of this group of stars, target selection will be done utilizing the dipolar mode visibility  $V_{\ell=1}^2$  [SCF<sup>+</sup>16b].

The mode visibility is defined as the ratio of the total power of a selected non-radial oscillation mode to the total  $\ell=0$  radial power (see e.g. [MEH+12, KDH+14, SCF+16b, MBP+17]). As the focus of this study revolves around  $\ell=1$  dipole modes, the mode dipole mode visibility is defined as follows

$$V_{\ell=1}^2 = \frac{A_{\ell=1}}{A_{\ell=0}},\tag{2.3}$$

where  $A_{\ell}$  is the sum of power amplitudes attributed to an oscillation mode. Stars with normal

dipolar mode amplitudes show higher mode visibilities  $V_{\ell=1}^2$  compared to those with suppressed modes across their spectrum. And since the partially suppressed stars still maintain some fraction of their dipolar mode amplitudes, their visibilities should exist in an intermediate region between the normal and suppressed stars. This can be seen in figures 2.6 and 2.7 where the stars KIC 6975038, KIC 8684542, and KIC 2018283 are highlighted and showcases that the dipole mode visibility  $V_{\ell=1}^2$  of the partially suppressed star KIC 6975038 is found between a normal red giant, KIC 8684542, and one that is fully suppressed, KIC 2018283.

To measure the visibilities  $V_{\ell=1}^2$ , the frequency regions that each oscillation mode occupies in the PSD follows the formalism of [SCF<sup>+</sup>16a] which defines the radial  $\ell=0$ , dipole  $\ell=1$ , quadrupole  $\ell=2$ , and octupole  $\ell=3$  modes as follows

$$\begin{split} \ell &= 0: \ \epsilon_p - 0.06 < (\nu/\Delta\nu \ \text{mod} \ 1) < \epsilon_p + 0.10 \\ \ell &= 1: \epsilon_p + 0.25 < (\nu/\Delta\nu \ \text{mod} \ 1) < \epsilon_p + 0.78 \\ \ell &= 2: \epsilon_p - 0.22 < (\nu/\Delta\nu \ \text{mod} \ 1) < \epsilon_p - 0.06 \\ \ell &= 3: \epsilon_p + 0.10 < (\nu/\Delta\nu \ \text{mod} \ 1) < \epsilon_p + 0.25 \end{split} \tag{2.4}$$

where  $\epsilon_p$  is the pure-pressure mode phase offset in the PSD. The segmentation of the PSD using these boundary conditions is seen in figures 2.3, 2.4, and 2.5 which helps to clearly illustrate the differences in the  $\ell=1$  region of the spectra when mixed modes are present (KIC 8684542), suppressed (KIC 2018283) and partially suppressed (KIC 6975038).

Figures 2.6 and 2.7 are a recreation of figure 4 in [SCF<sup>+</sup>16a] (see figure 2.2) using 3574 out of their 3611 Kepler red giants; the smaller sample I take here is plainly because the asteroseismic calibrated power spectra densities for all targets were not available to me at the time. Figure 2.6 shows the dipole mode visibility  $V_{\ell=1}^2$  as it is calculated in [SCF<sup>+</sup>16a, SCF<sup>+</sup>16b] while figure 2.7 shows the dipole mode visibility  $V_{\ell=1}^2$  with the application of a Gaussian weighted average.

In section 2.2 it is noted that the oscillation power excess is approximated by a Gaussian envelope centered around  $\nu_{max}$ , with that, the choice was made to use the fitted parameters from *apollinaire* [BGB<sup>+</sup>22] to create an estimate of this envelope and apply it to the power spectra following as

$$PSD_{P(\nu)} = \frac{\sum_{i=1}^{n} PSD_{i} \cdot P(\nu)_{i}}{\sum_{i=1}^{n} P(\nu)_{i}},$$
(2.5)

where  $P(\nu)_i$  is the Gaussian power at the frequency  $\nu$  from equation 2.2. Equation 2.5 states that the Gaussian applied PSD,  $PSD_{P(\nu)}$ , is formed by applying the weighted average of the Gaussian for all frequency points i such that  $i \in [0, n]$ .

It must be noted that figures 2.6 and 2.7 zoomed in subsets of the [SCF<sup>+</sup>16a] sample as, for my estimations, there exists outliers with visibility estimates orders of magnitude larger and smaller than the main grouping of the sample. The abnormal visibility of these outliers may have been due to contamination sources like a bright nearby star causing peaks that fall within the frequency regions of  $\ell=0$  and/or  $\ell=1$ . In figures 2.6 and 2.7 there are two significant features, one being a branching of the visibilities  $V_{\ell=1}^2$  into two distinct populations for targets with  $\nu_{max}\gtrsim 60\mu{\rm Hz}$ , and the other being a downwards sloping of  $V_{\ell=1}^2$  values for targets with  $\nu_{max}\gtrsim 125\mu{\rm Hz}$ .

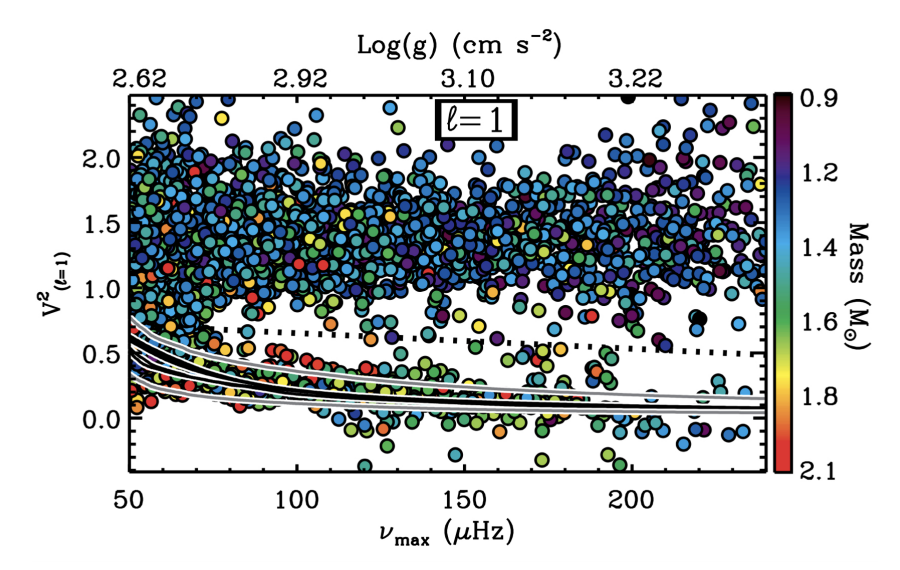


Figure 2.2: Extracted from [SCF<sup>+</sup>16a] figure 4, the dipole mode visibilities  $V_{\ell=1}^2$  for 3611 Kepler red giants are plotted against their frequency at maximum power  $\nu_{max}$ . The colors indicate the stellar mass in solar mass units  $\mathrm{M}_\odot$ , and are scaled following the color bar on the right of the figure. The dotted line is adopted from [SCF<sup>+</sup>16b] and separates the stars with normal stars from those showing suppressed dipole mode amplitudes. The black lines are showing the estimated visibilities from stellar models for a range of stellar masses (1.1, 1.3, 1.5, 1.7, 1.9 [ $\mathrm{M}_\odot$ ]) wherein the average lifetime of a mode is 20 days following the peakbagging analysis of [CDG15] section 2. The gray lines are similarly showing the estimated visibilities from a  $1.7\mathrm{M}_\odot$  stellar model, but with the average mode lifetime just 10 days, and an average mode lifetime just under 40 days. The depiction of varying mode lifetimes shows the slight dependence of  $V_{\ell=1}^2$  on these lifetimes with the gray lines being distinct, while highlighting the lack of dependence on the stellar mass for the black lines which mostly overlap one another.

The branching is consistent with visibility  $V_{\ell=1}^2$  estimates in [MEH+12, KDH+14, SCF+16b, SCF+16a] and shown in figure 2.2 who attribute this behaviour to a high degree of p- and g-mode coupling creating mixed modes with a high mode mass, therein making it difficult to visualize the tree resultant low amplitudes that reach the surface [MEH+12, KDH+14], and notably in [SCF+16b] that cites magnetic trapping of the mixed modes introduced in [FCS+15]. With an internal magnetic field mainly affecting the dipolar mixed modes, as they travel close to the stellar core, the suppression of these modes in the PSD is the result of a magnetic greenhouse affect wherein oscillation mode energy is trapped in the stellar core and unable to continue propagation to the surface [FCS+15].

On the contrary, this overall decrease in  $V_{\ell=1}^2$  when  $\nu_{max}\gtrsim 125\mu{\rm Hz}$  differs from the results of [MEH+12, KDH+14, SCF+16a, SCF+16b] and cannot be seen in figure 2.2 from [SCF+16a]. Attaining this feature after conducting the estimate of the mode visibility  $V_{\ell=1}^2$  prompted further investigation to determine the discrepancy; the visibilities  $V_{\ell=1}^2$  were recalculated without the application of the Gaussian weighted average onto the oscillation power excess as this approach is not classical. This approach yielded similar results in terms of the overall sloping of the visibilities  $V_{\ell=1}^2$ , showing a different scaling of the values that appears to maintain their relative values to one another. Further investigation of this behaviour will need to be explored in follow-up studies. For the purposes of this work, the partially suppressed star has an intermediate visibility  $V_{\ell=1}^2$  as expected; the confirmation of this will inform future searches for more of these unique red giants.

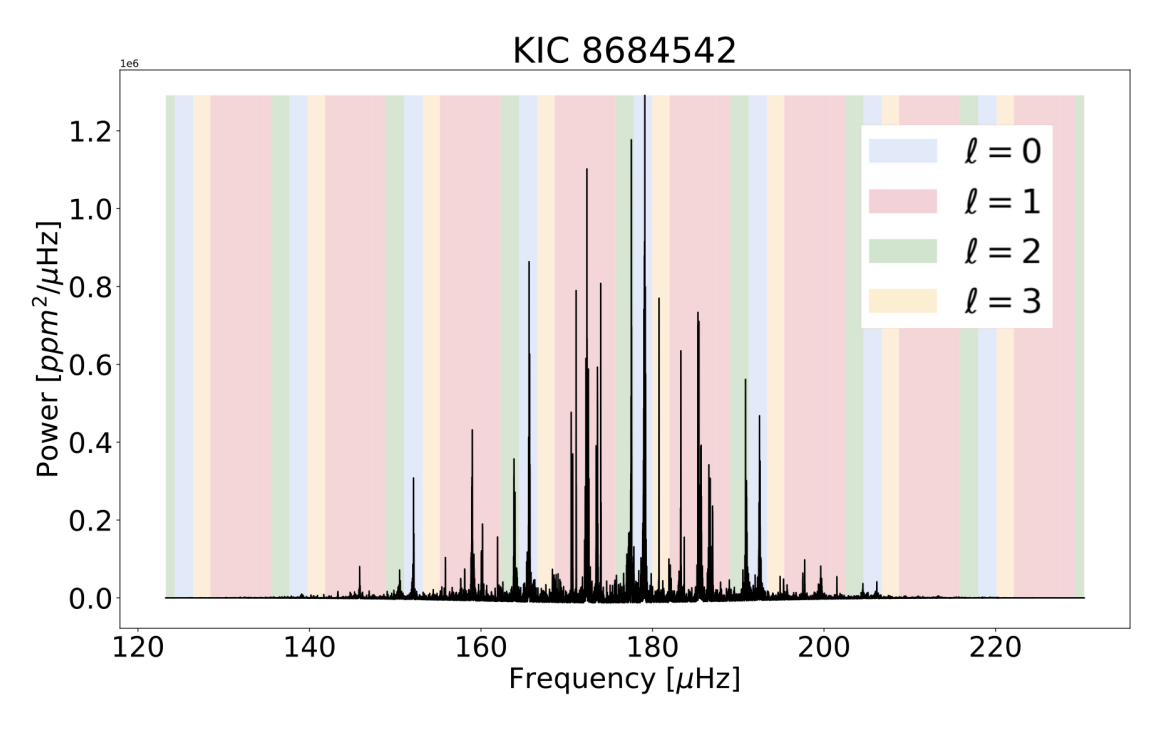


Figure 2.3: PSD of the sample star KIC 8684542 showing the original data in black segmented into the regions of  $\ell=0,1,2,3$ , following the masking formalism of [SCF+16a, SCF+16b] shown in equation 2.4. The colors are attributed to the oscillation modes as follows:  $\ell=0$  is blue,  $\ell=1$  is red,  $\ell=2$  is green, and  $\ell=3$  is yellow. In this work, KIC 8684542 is representative of a "normal" red giant presenting with dipole mixed modes. The mixed mode characteristic where the power density of a single  $\ell=1$  mode being redistributed within this region is visible in comparison to the mostly singular peaks of  $\ell=0,2,3$ .

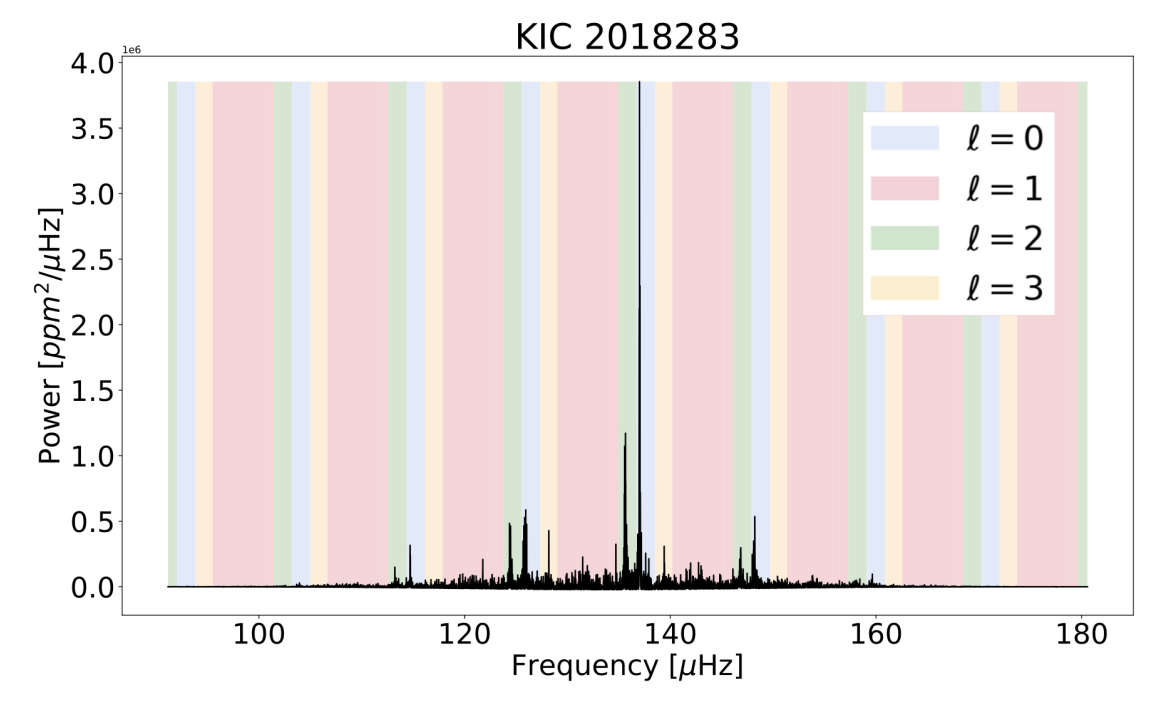


Figure 2.4: PSD of the sample star KIC 2018283, with the same segmentation of mode frequency regions as in figure 2.3. Of note for this star is the suppression of the dipole mixed mode  $\ell=1$  in the red regions; shown in [SCF+16b] figure 1. In this work, KIC 2018283 will serve as the fully suppressed star example.

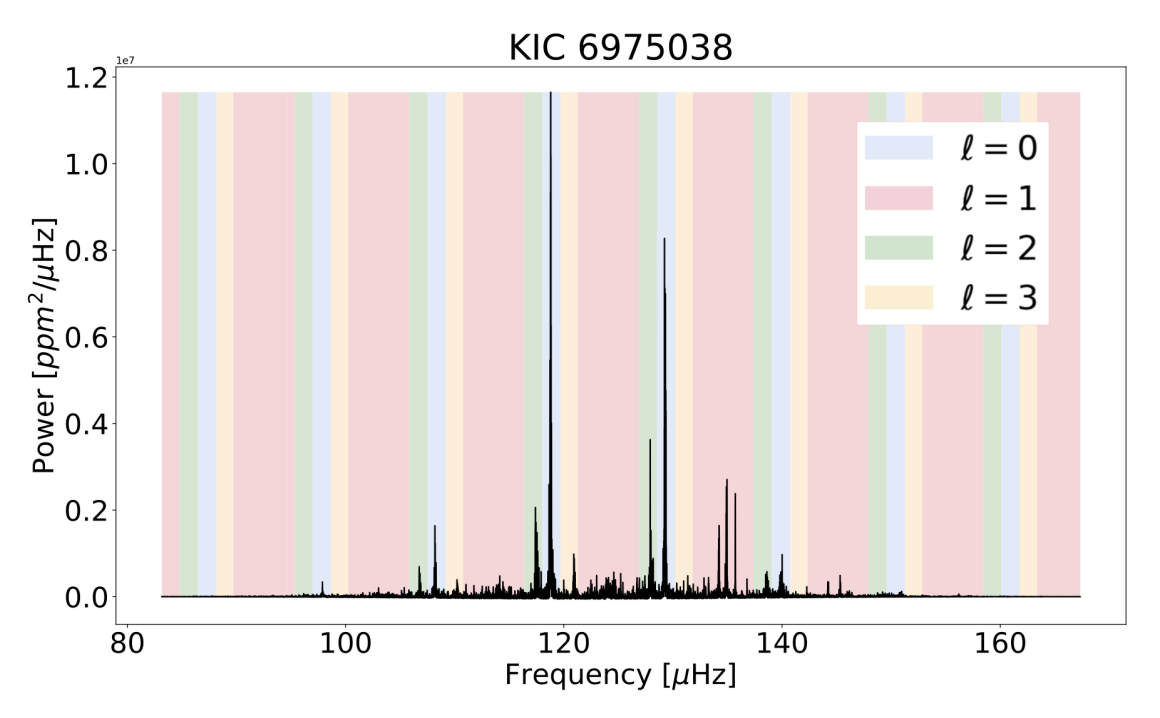


Figure 2.5: PSD of the sample star KIC 6975038, with the same segmentation of mode frequency regions as in figures 2.3 and 2.4. The notable feature that makes this target the main star of this work is the partially suppressed dipole mode amplitudes seen in the red  $\ell=1$  regions. Noted for the unusual partial suppression in [MBP+17], [MPB+17], [Loi20], [DLBL23], [ROM23], and [AT24] this star was reported by [DLBL23] to have a magnetic field strength around 180 kilo-Gauss in the hydrogen burning shell surrounding the core. The suppression of low frequency dipole  $\ell=1$  mixed modes is attributed to the field, although the appearance of high frequency  $\ell=1$  modes requires further investigation of magnetic signatures on this star, namely frequency shifts.

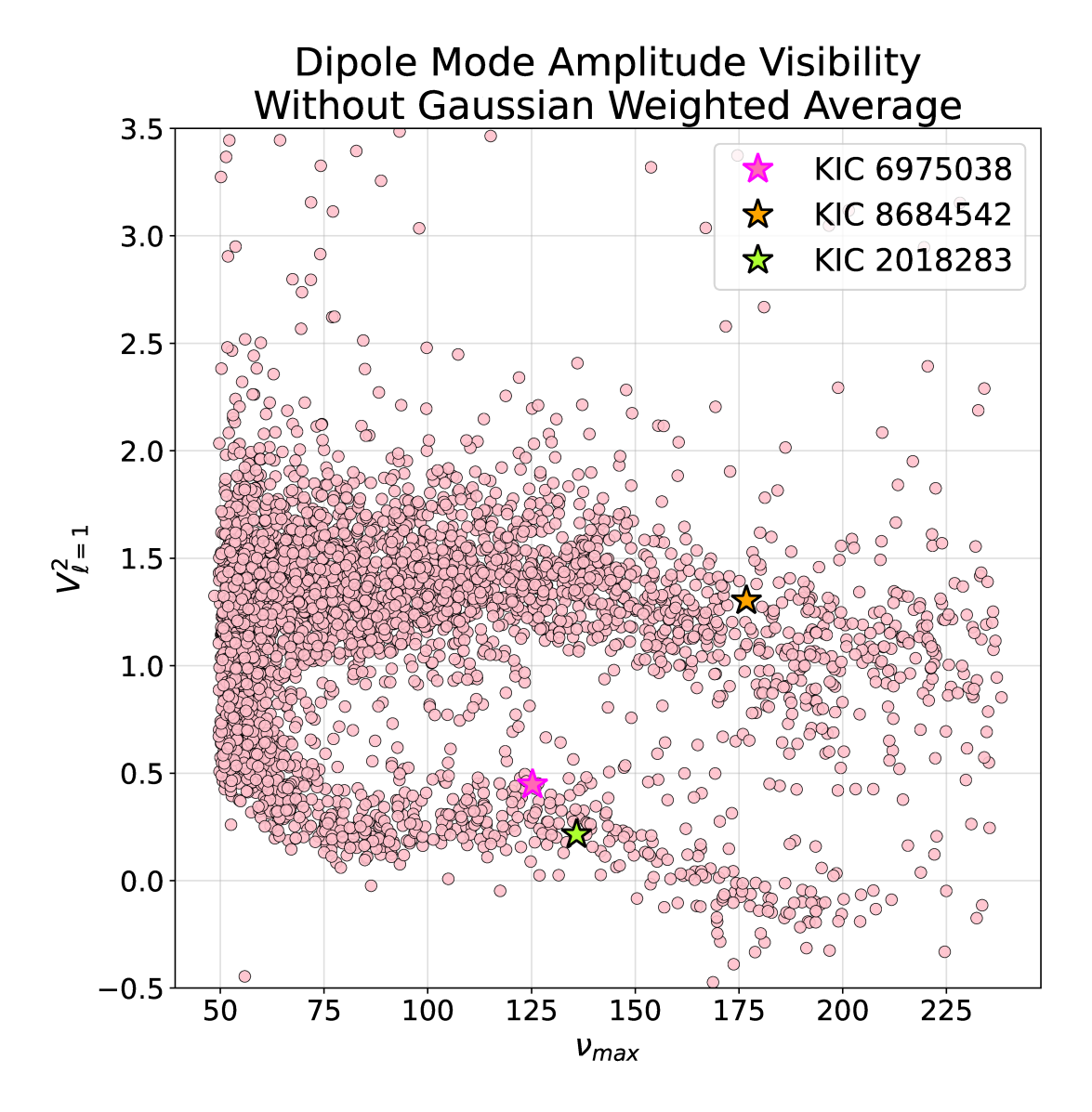


Figure 2.6: Dipole mode visibilities  $V_{\ell=1}^2$  calculated in this study using the oscillation mode regions in 2.4. KIC 6975038, KIC 8684542, and KIC 2018283 are highlighted as star points in bright pink, orange, and green respectively. KIC 8684542 resides in the "normal" region of visibility around 1.35 [SCF+16a] with  $V_{\ell=1}^2\approx 1.30$ . KIC 2018283 resides in the suppressed mode region, around 0.5 or down to zero for the least evolved stars, with  $V_{\ell=1}^2\approx 0.21$ . KIC 6975038 resides in the intermediate region between the two previous stars, as we expect for a star with only partially suppressed mode amplitudes, with  $V_{\ell=1}^2\approx 0.45$ .

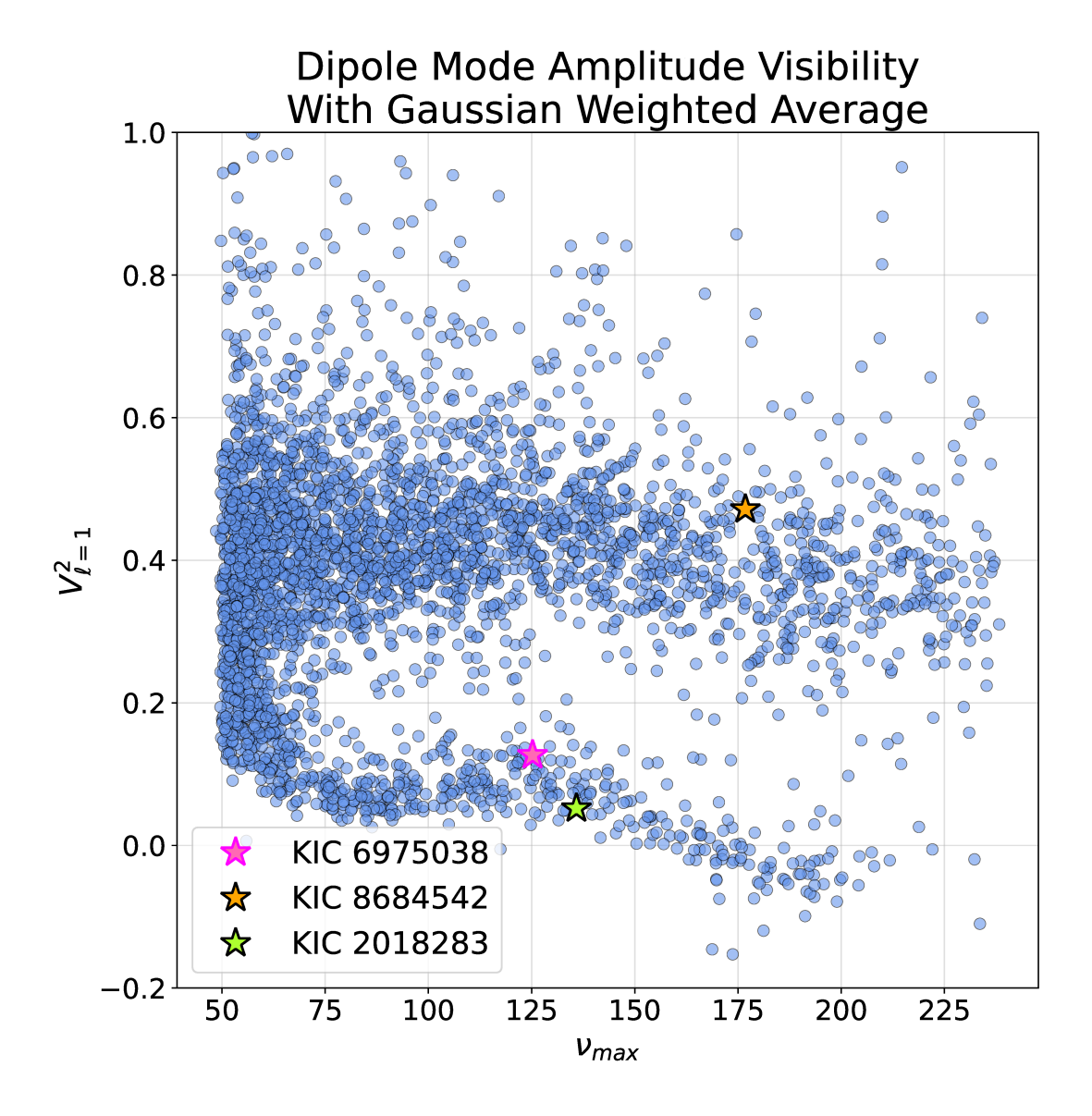


Figure 2.7: Dipole mode visibilities  $V_{\ell=1}^2$  calculated in this study using the oscillation mode regions in 2.4; differently from figure 2.6, here the Gaussian weighted average of figure 2.2 has been multiplied to each star. The positions relative to one another remain the same for the highlighted stars KIC 6975038, KIC 8684542, and KIC 2018283, shown as star points in bright pink, orange, and green respectively. KIC 8684542 resides on the "normal" branch of visibility with  $V_{\ell=1}^2 \approx 0.47$ . KIC 2018283 resides in the suppressed mode region with  $V_{\ell=1}^2 \approx 0.05$ . KIC 6975038 resides in the intermediate region between the two previous stars with  $V_{\ell=1}^2 \approx 0.13$ .

# CHAPTER 3

#### **Methods**

#### 3.1 PSD Modeling & Additional Relevant Parameters

Modeling of the power spectra involves using an adapted version of the open-source *Python* stellar modeling code *sloscillations\_ISTA* (Desai et al., in prep), originally developed by [KCN+19] and named *sloscillations*. This package is designed to model the stellar power spectra of red giants using fundamental asteroseismic parameters and scaling relations to recreate oscillation mode amplitudes. The modified version of the package used in this work includes the addition of internal magnetism, allowing for this study to investigate if characteristic magnetic frequency shifts are present in the dipole mixed modes of the partially suppressed star.

To model the spectra with *sloscillations\_ISTA* (Desai et al., in prep), the pure-pressure mode eigenfrequencies are estimated via the second-order asymptotic expression [Tas80] as follows

$$\nu_{p,\ell=1} = \Delta\nu \left( n_p + \frac{\ell}{2} + \epsilon_p - \delta_{01} + \frac{\alpha_\ell}{2} \left( n_p - \frac{\nu_{max}}{\Delta\nu} \right)^2 \right), \tag{3.1}$$

where  $\mathbf{n_p}$  is the radial order of the pressure modes in the range  $\mathbf{n_p} \in [5:20]$  for red giants,  $\epsilon_{\mathbf{p}}$  is the pure-pressure mode phase offset which is assumed to follow the scaling law  $\epsilon_{\mathbf{p}} = 0.634 + 0.63 \log_{10}(\Delta \nu)$  [MBG+11],  $\alpha_{\ell}$  is the curvature in the radial mode oscillation pattern following  $\alpha_{\ell} = 0.015 \Delta \nu^{-0.32}$  [MMB+13],  $\delta_{01}$  is the small frequency separation of  $\ell=1$  and the midpoint between the surrounding  $\ell=0$  modes, following the scaling law  $\delta \nu_{01} = -0.056 - 0.002 \log_{10}(\Delta \nu)$  [MBG+11]. Additionally,  $\mathbf{n_{max}} = \frac{\nu_{max}}{\Delta \nu} - \epsilon_{\mathbf{p}}$  is the non-integer radial order  $\mathbf{n}$  closest to  $\nu_{max}$ .

With the onset of mixed modes in red giant stars, with varying ratios of characteristics from both pressure and gravity waves, their dipole mode eigenfrequencies are estimated following  $[MGB^+12b]$ 

$$\nu_{pg,\ell=1} = \nu_{p,\ell=1} + \frac{\Delta\nu}{\pi} \arctan\left[q \tan\left[\pi \left(\frac{1}{\Delta\Pi_1 \nu_{pg,\ell=1}} - \epsilon_g\right)\right]\right]$$
(3.2)

where  $\Delta\Pi_{\ell=1}$  is the asymptotic period spacing of the gravity-dominated mixed modes and follows a tight relationship with  $\Delta\nu$  scaling as  $\Delta\Pi_{\ell=1}=60+1.7\Delta\nu$  in [KHH23],  $\epsilon_{\rm g}$  is the gravity mode offset, and  ${\bf q}$  is the coupling factor between the pure-pressure and pure-gravity modes [MPB<sup>+</sup>17]. Additionally, q=0 indicates no coupling while q=1 indicates maximum coupling of the modes. The parameter  ${\bf q}$  is expressed using the implicit asymptotic relation of mixed modes following the work of [Shi79] and [UOA<sup>+</sup>89] by ways of combing the phases of pressure,  $\theta_p$ , and gravity-wave,  $\theta_g$ , contributions to the mixed modes as

$$\tan \theta_p = q \tan \theta_g; \tag{3.3}$$

as the expression in equation 3.3 cannot be solved analytically, a numerical root finding algorithm is used to find frequencies satisfying the equation where,

$$\theta_p\left(\nu_{pg,\ell=1}\right) = \pi \frac{\nu_{pg,\ell=1} - \nu_{p,\ell=1}}{\Delta\nu} \tag{3.4}$$

and,

$$\theta_g(\nu_{pg,\ell=1}) = \pi \frac{1}{\Delta \Pi_{\ell=1}} \left( \frac{1}{\nu_{pg,\ell=1}} - \frac{1}{\nu_{g,\ell=1}} \right).$$
 (3.5)

The parameters  $\nu_{p,\ell=1}$  and  $\nu_{q,\ell=1}$  are the frequencies of the pure pressure and gravity modes.

As there are varying ratios of p-and g-mode contributions to mixed modes, the nature of the mixed mode, that is, the dominating contributor between p-and g-modes, can be represented with mode inertia [GMM $^+$ 13]; the ratio of the mode inertia in the radiative interior and the total mode inertia is described by the function  $\zeta\left(\nu_{pg,\ell=1}\right)$  (introduced by [GMM $^+$ 13] and used in subsequent work by [BBB $^+$ 14] and [DBB $^+$ 15]) following

$$\zeta\left(\nu_{pg,\ell=1}\right) = \left(1 + \frac{q}{\mathcal{N}} \frac{1}{q^2 \cos \theta_p^2 + \sin \theta_p^2}\right)^{-1},\tag{3.6}$$

where  $\mathcal{N} = \Delta \nu / (\nu^2 \Delta \Pi_{\ell=1})$  is the number of mixed modes per  $\Delta \nu$  interval, describing the density of gravity modes compared to the pressure modes. For gravity-dominated mixed modes, equation 3.6 will tend to unity, while for pressure-dominated mixed modes, 3.6 will tend to zero.

Modulations to the dipole mixed modes arise from stellar differential rotation of the convective envelope and radiative interior which induce splitting of the mode frequencies  $\delta\nu_{rot,env}$  and  $\delta\nu_{rot,int}$ , respectively; both  $\delta\nu_{rot,env}$  and  $\delta\nu_{rot,int}$  are initial user input parameters in the PSD model and will remain constant during the fitting to be discussed in section 3.2. The function in equation 3.6 is used to describe the rotational splitting of mixed modes as a function of the mean rotational splittings resulting from pure gravity modes in the radiative interior  $(\delta\nu_{rot,int})$  and pure pressure modes in the convective envelope  $(\delta\nu_{rot,env})$ , expressed as  $\delta\nu_{rot} = \zeta\delta\nu_{rot,int} + (1-\zeta)\delta\nu_{rot,env}$ . For gravity-dominated mixed modes that are predominantly sensitive to the interior rotation perturbation, it is reasonable to assume that the envelope rotation effects  $(\delta\nu_{rot,env})$  are negligible [MGB<sup>+</sup>18] and the rotational splitting can be approximated as follows

$$\delta\nu_{rot} = \delta\nu_{rot,int}\zeta,\tag{3.7}$$

where  $\delta \nu_{{\bf rot,int}}$  is taken to be half of the rotation frequency of the radiative interior region [LDL<sup>+</sup>23] such that

$$\delta\nu_{rot,int} = \frac{\omega_{int}}{2}. ag{3.8}$$

For a dipole mixed mode with azimuthal orders  $m=0,\pm 1$ , the observed gravity-dominated frequencies have a dependence on m following  $\nu_{\rm obs_m}=\nu_{\rm m=0}+\delta\nu_{\rm rot_m}$  where  $\nu_{m=0}$  is the unperturbed mixed mode frequency at m=0, and

$$\delta\nu_{rot_m} = m\delta\nu_{rot,int}\zeta,\tag{3.9}$$

the resulting affect from the interior rotation on the dipole mixed modes is a symmetric frequency splitting of the  $m=\pm 1$  components around the unperturbed m=0 component of the mode, illustrated in figure 3.1.

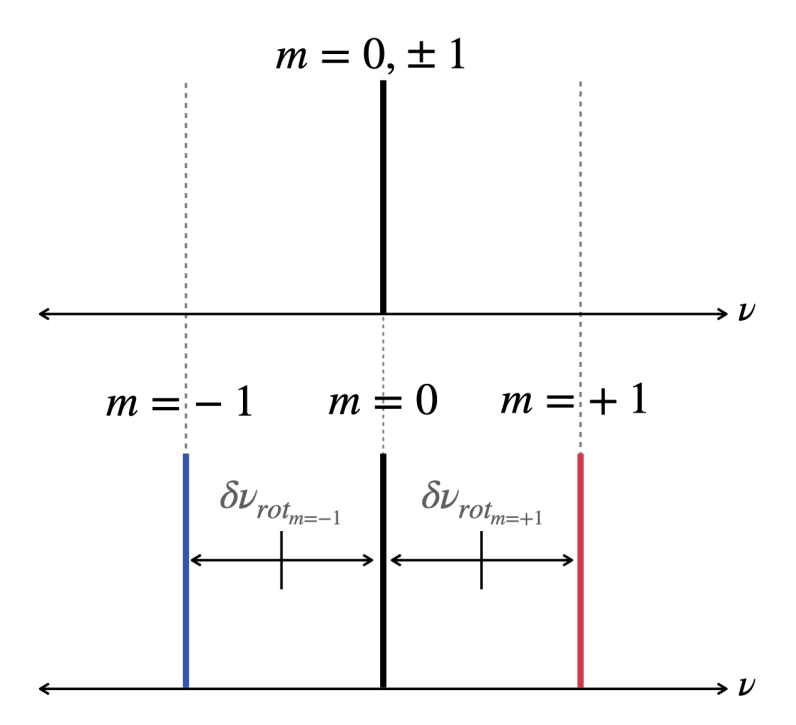


Figure 3.1: Symmetric splitting of the dipole mixed mode frequencies into the azimuthal components  $m=0,\pm 1$  following equations 3.7 and 3.9. The top panel of the figure shows the dipole mixed mode without rotational perturbation, while the bottom illustrates the splitting of the modes in the rotating case showing that m=0 remains stationary while  $m=\pm 1$  will shift in equal and opposite directions.

The aforementioned key magnetic signature wherein the dipole mixed modes are shifted to higher frequencies, is described by the parameter  $\delta \nu_{mag,g}(\nu)$  following the formalism shown in [Bug22] as

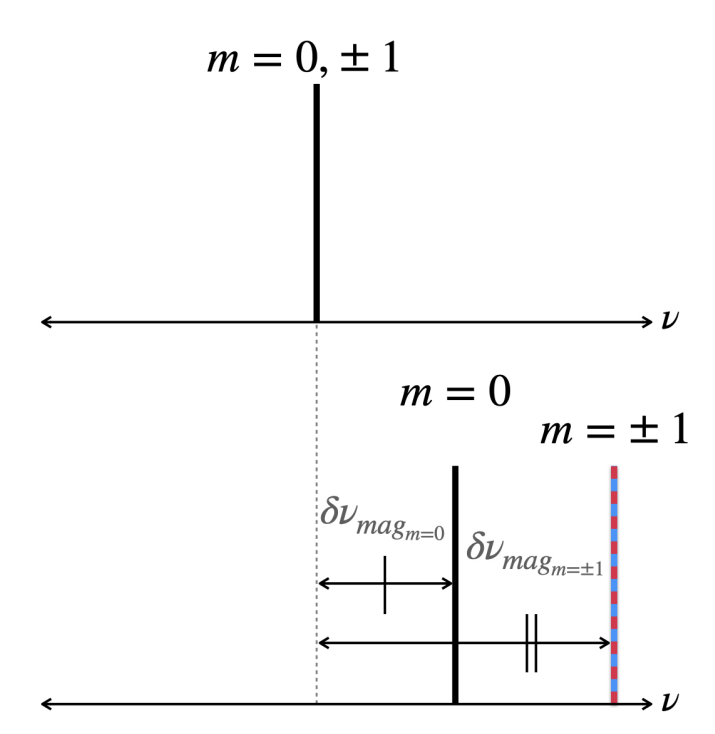


Figure 3.2: Asymmetric magnetic splitting of the dipole mixed mode frequency azimuthal components  $m=0,\pm 1$  following equation 3.10. The top panel is identical to that in figure 3.1 showing the dipole mixed mode, in this case without magnetic perturbation, while the bottom panel illustrates the splitting of the mode caused by magnetic perturbation. It can be seen here that the m=0 component of the mode shifts to higher frequencies by half as much as the  $m=\pm 1$  components which shift by the same amount.

$$\delta\nu_{mag_m} = m^*\zeta\delta\nu_{mag,g}(\nu) = m^*\zeta\frac{AB_0^2}{\nu^3}, \ m^* = \frac{|m|+1}{2},$$
 (3.10)

where  ${\bf A}$  is a normalization factor dependent on the field topology and stellar structure (see [Bug22] for further details on the terms contained within  ${\bf A}$ ),  ${\bf B_0}$  is the amplitude of the magnetic field, and the term  $\delta\nu_{\rm mag,g}(\nu)$  is the magnetic perturbation for pure g-modes. Of note here is that the function  $\zeta$  in equation 3.10 scales the amount of pure g-mode magnetic perturbation according to g-mode contribution in the mixed mode, of which the function  $\zeta$  describes. For red giant stars, magnetic perturbations on dipole mixed mode frequencies shift all 3 azimuthal components, unlike rotation, such that the m=0 component of the mode will shift half as much as the  $m=\pm 1$  components which can be seen illustrated in figure 3.2. Of note for the magnetic splitting is the  $1/\nu^3$  dependence, meaning that magnetic shifting will be strongest for mixed modes at low frequencies; in the case of partially suppressed red giant stars, this dependence may cause difficulty in detecting magnetic perturbations with few  $\ell=1$  intervals which reside at relatively high frequencies in the respective PSD's, as is the case for KIC 6975038. The magnetic shifting parameter,  $\delta\nu_{mag,g}(\nu)$ , will herein be denoted as  $\delta\nu_{\rm mag}$ .

As the magnetic shifting of the dipole mixed modes is dependent on the azimuthal term m, magnetic perturbations introduce an asymmetry to the modes; studied in [LDBL22] and explored in [BPM $^+$ 21], the asymmetry parameter a follows

$$a = \frac{\nu_{m=1} + \nu_{m=-1} - 2\nu_{m=0}}{1/3 \left(\delta \nu_{mag,m=1} + \delta \nu_{mag,m=0} + \delta \nu_{mag,m=-1}\right)},$$
(3.11)

where  $\nu_m$  is the the frequency of the mixed mode with some m. With a range of  $a \in [-\frac{1}{2},1]$  (see [LDBL22] supplementary material for a detailed explanation), the asymmetry parameter a allows for better understanding of the magnetic field topology as the minimum corresponds to the radial component of the magnetic field being concentrated around the stellar pole, while the maximum corresponds to the radial component of the magnetic being concentrated around the stellar equator (eg., [LDBL22, MB23]).

#### 3.2 Bayesian Fitting

Bayesian fitting of the model parameters  $\Delta\nu$ ,  $\delta\nu_{mag}$ ,  $\delta\nu_{rot}$ ,  $\theta_{inc}$ , a, q,  $\epsilon_{p}$ ,  $\Delta\Pi_{\ell=1}$ , was conducted using a Bayesian fitting code called *Bayes\_sloscillations\_ISTA* (Desai et al. in prep). The Bayesian fitting process in the case of this study follows that *sloscillations\_ISTA* generates a PSD model using equations listed in section 3.1, *Bayes\_sloscillations\_ISTA* (Desai et al. in prep) then compares the the PSD model to the original PSD data following what is defined in the code the loss function,

Bayesian Mod	lel Parameters
Parameter to be Fit	Walkers Initial Distribution
	Sampling Range
$\Delta  u  [\mu {\sf Hz}]$	$\Delta \nu - 0.6 < \Delta \nu < \Delta \nu + 0.6$
$\delta  u_{mag} \ [\mu  extsf{Hz}]$	$0 < \delta \nu_{mag} < 0.2$
$\delta  u_{rot}  [\mu {\sf Hz}]$	$0 < \delta \nu_{rot} < 0.8$
$\theta_{inc}$ [°]	$30^{\circ} < \theta_{inc} < 60^{\circ}$
a [unitless]	-0.5 < a < 1
q [unitless]	0 < q < 1
$\epsilon_g$ [unitless]	$-0.5 < \epsilon_g < 0.5$
$\epsilon_p$ [unitless]	$-0.5 < \epsilon_p < 0.5$
$\Delta\Pi_{\ell=1}$ [seconds]	$50 < \Delta \Pi_{\ell=1} < 150$

Table 3.1: List of the model parameters involved in the Bayesian fitting in Bayessloscillations\_ISTA (Desai et al. in prep.). All parameters except for  $\Delta\nu$  are sampled from a uniform distribution bounded by the ranges given in column 2.  $\Delta\nu$  is sampled from a Gaussian distribution with a standard deviation  $\sigma=0.15$ ; the reason for this narrow sampling range is to because the  $\Delta\nu$  values for Kepler red giants are well studied and well constrained, so the parameter space exploration does not need to be large.

loss = 
$$-\frac{1}{2} \sum_{i=1}^{n} \left[ \frac{(PSD_{model_i} - PSD_{real_i})^2}{0.02^2} + \log(2\pi(0.02^2)) \right].$$
 (3.12)

The goal of the Bayesian fitting is to reduce the chosen loss function in equation 3.12, optimizing parameters being fit such that the model closely matches the real data at each index of power, i. The parameters being fit during this process follow an MCMC parameter space exploration wherein the prior values are sampled from a continuous uniform distribution,

#### 3. Methods

over the range listed in table 3.1 column 2, to establish the 200 walkers. An exception is made for the parameter  $\Delta\nu$  which is sampled from a Gaussian distribution with  $\sigma=0.15$ ; this is done because  $\Delta \nu$  is a fundamental asteroseismic parameter heavily impacting the observed behaviour of the oscillation modes, as such, a narrow parameter space exploration is established to tightly constrain it. As the walkers explore the parameter space within the boundaries of table 3.1 column 2, a new PSD model is generated and again compared to the real data PSD. The movement or updating of the coordinates of the walkers in the parameter space follows the emcee.moves function KDEMove where KDE stands for Kernel Density Estimation; the KDE algorithm is an efficient ensemble sampling algorithm that allows for parallelized updates of all parameters (see [FHLG13] for more details on MCMC ensemble sampling). It is in this way, that is, the ensemble parameter updates, that the Bayesian fitting process from Bayes\_sloscillations\_ISTA (Desai et al. in prep) is capable of constraining the magnetic field properties as the parameters are simultaneously evaluated and updated to obtain a model that best fits the comparative real data. Again, the goal of this process is to find a model such that the difference between the model and the real data is minimized and the parameters converge on the values that create the best fitting model.

# CHAPTER 4

### Results

#### 4.1 KIC 8684542: A "Normal" Red Giant

To test the performance of <code>Bayessloscillations\_ISTA</code> (Desai et al. in prep.) before deploying it on the partially suppressed star, we first conduct the Bayesian fitting for the "normal" red giant star, KIC 8684542, that is, a red giant star reported to have magnetic frequency shifts (see <code>[LDL+23]</code> and <code>[HON+24]</code>) of the dipole mixed modes, but not any dipole mode suppression. Figure 4.1 shows the resulting model created with the fitted parameters in red, while the original data is plotted in black. The pure acoustic  $\ell=0$  mode is well identified across the spectrum and highlighted with a purple star, while the  $\ell=2$  oscillation modes become slightly shifted away from the data at higher frequencies. The notable feature in figure 4.1 is the complex  $\ell=1$  dipole mixed mode pattern. Although this star is denoted as a "normal" red giant star, it has a dipole mixed mode pattern that is difficult to characterize as it is inclined at  $71.9^{+18}_{-7}$  degrees [°] <code>[GMMC21]</code>. Meaning that at such a high inclination, such as is depicted in figure 1.1, the splitting of the mixed modes into the azimuthal components  $m=0,\pm 1$  become difficult to resolve, making it difficult to characterize both magnetic and rotational perturbations from the spectra.

As such, although the mixed mode pattern in this test star is difficult to characterize, we will still utilize the *Bayessloscillations\_ISTA* (Desai et al. in prep.) fitting on the stellar power spectra for a star at intermediate inclinations; in the future, the *sloscillations\_ISTA* model will need to be adjusted to accommodate these types of stars, and this current work will ideally serve to identify limitations of the model to plan for creating solutions. The question now arises whether characterization of magnetic perturbations of KIC 6975038 will be possible if the inclinations are outside of the intermediate range of  $[30^{\circ}-60^{\circ}]$ , as an estimate of the inclination for this star has yet to be reported.

The parameters from the Bayesian fitting of KIC 8684542 are listed in table 4.1. The difficulty in constraining the inclination angle  $\theta_{inc}$  was already mentioned, and the resultant fit of  $\theta_{inc}=44.225^{+8}_{-8} [^{\circ}]$ , which is outside of the error bars for the value reported in [GMMC21], also highlights this point. Additional parameters from the fitting procedure including  $\delta\nu_{mag}, \epsilon_g, \epsilon_p$  and  $\Delta\Pi_{\ell=1}$  are also outside of the error bars for their respective values reported in studies from [MPB+17], [GMM+18], [LDL+23], and [HON+24]; these discrepancies can be attributed to the difficulty in modeling the PSD of a red giant presenting with a complex mixed mode pattern that is reported to have both magnetic and rotational shifting, in addition to a high

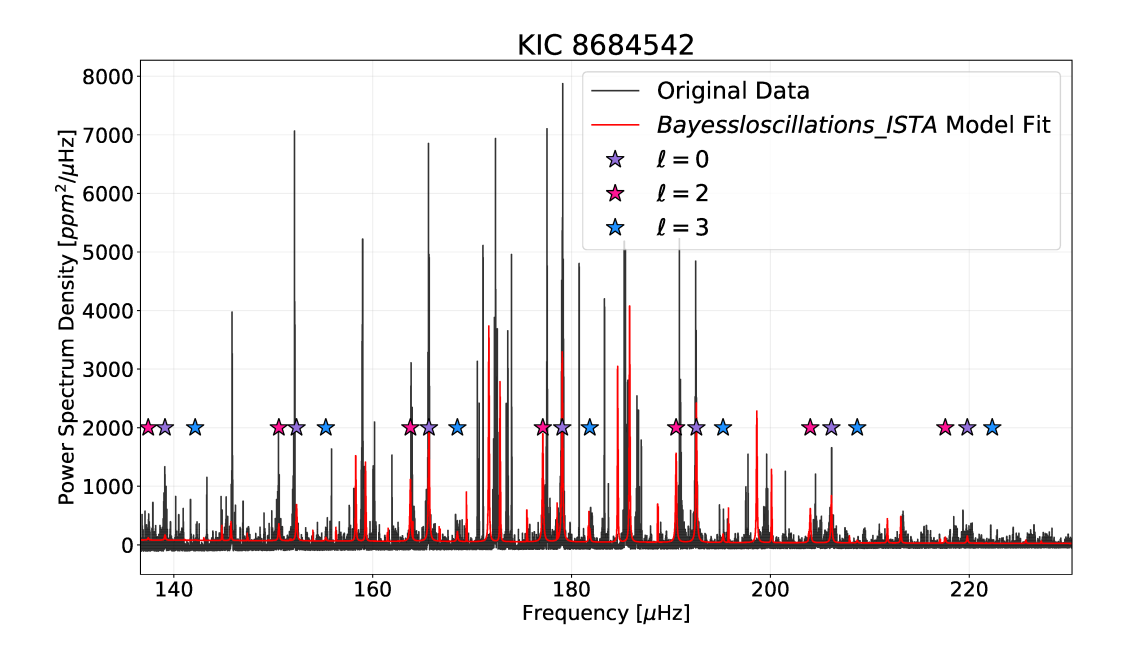


Figure 4.1: The resultant PSD of KIC 8684542 is shown in red plotted over the original data in black. For ease in locating the  $\ell=1$  dipole mode regions, the  $\ell=0,2,3$  modes are highlighted with star markers in the colors purple, pink, and blue respectively, such that the  $\ell=1$  oscillation modes reside between the  $\ell=2$  and  $\ell=3$  modes.

inclination that increases the difficulty of constraining the two previously mentioned parameters as the m=0 component of the mixed modes becomes less visible.

For future work, a more robust testing method for the performance of <code>Bayessloscillations\_ISTA</code> (Desai et al. in prep.) would be to start with conduction Bayesian fitting of a well characterized red giant star of intermediate inclination that has not been reported to have mixed modes; for a star such as this, fitting for the parameters  $\delta\nu_{mag}, a, q, \epsilon_g$ , and  $\Delta\Pi_{\ell=1}$  can either be turned off and fixed to values appropriate for no coupling of the p-and g-modes, or they can remain as fit parameters to test if the fitting procedure can achieve the aforementioned appropriate values for no coupling. The next step would be to model another well characterized red giant at an intermediate inclination, this time one presenting with mixed modes that has not been reported as displaying magnetic frequency shifts; a similar process as previously detailed for fitting the PSD of this star can be conducted, both with and without fixing the parameters  $\delta\nu_{mag}$  and a, again to check if the model can converge to appropriate values for no internal magnetic activity detection.

#### 4.2 KIC 6975038

### 4.2.1 Sigmoid Profile of a Partially Suppressed Red Giant

The characteristic feature for a partially suppressed red giant is the absence and sharp reappearance of the  $\ell=1$  mode amplitudes around  $\nu_{max}$ , differing from the dipolar mode amplitude profile of a "normal" red giant showing mixed modes. Based on the unusual nature of this mode suppression feature, the novelty of this work will be to model the dipolar power spectra of partially suppressed red giants with a sigmoid profile as follows

Fit Parameters				
Parameter	KIC 8684542			
$\Delta  u  [\mu {\sf Hz}]$	$13.459^{+0.024}_{-0.016}$			
$\delta  u_{mag} \ [\mu  ext{Hz}]$	$0.060^{+0.048}_{-0.035}$			
$\delta  u_{rot}  [\mu {\sf Hz}]$	$0.088^{+0.147}_{-0.060}$			
$\theta_{inc}$ [°]	$44.225^{+8}_{-8}$			
a [unitless]	$0.206^{+0.365}_{-0.366}$			
q [unitless]	$0.081^{+0.018}_{-0.013}$			
$\epsilon_g$ [unitless]	$-0.093^{+0.233}_{-0.212}$			
$\epsilon_p$ [unitless]	$0.304^{+0.016}_{-0.023}$			
$\Delta\Pi_{\ell=1}$ [seconds]	$99^{+31}_{-1}$			

Table 4.1: List of the fit model parameters from *Bayessloscillations\_ISTA* (Desai et al. in prep.) for KIC 8684542 including the respective errors measured as the difference between the mean and 16th and 84th percentiles from the resultant MCMC chain of walkers.

$$S = \frac{1}{1 + \exp(-a_{horiz.} \cdot (\nu - \nu_i - h_{horiz.}))}, \nu_i = \nu_{max}$$

$$= \frac{1}{1 + \exp(\nu - \nu_{max})}$$
(4.1)

where  $a_{horiz}$  controls the horizontal stretch or compression, and  $h_{horiz}$  is the horizontal shift away from the inflection point  $\nu_i$  of the function set at  $\nu_{max}$ . Fixing  $\nu_i$  at  $\nu_{max}$  for all targets is done because the currently identified targets exhibit mode suppression at frequencies below  $\nu_{max}$  (see figure 2.5). Additionally, the sigmoid profile reduces to smaller expression in equation 4.1 when the following parameters are set to constants:  $a_{horiz} = -1$  and  $h_{horiz} = 0$ ; since the variable of the sigmoid function have not yet been implemented as a fitting parameter in  $Bayessloscillations\_ISTA$  (Desai et al. in prep.), these parameters are fixed and the same Sigmoid is applied at each iteration of the fitting process. The decision to model the  $\ell=1$  partial mode suppression with a sigmoid profile was made because application of the sigmoid can effectively suppress low frequency amplitudes to near zero values, while still allowing for close to no mode suppression at high frequencies. In the future, if partially suppressed targets are identified with more diverse suppression profiles, the parameters  $a_{horiz}$  and  $a_{horiz}$  can be used to modulate the profile accordingly.

The process of modeling the power spectra density of a partially suppressed red giant requires isolating the  $\ell=1$  component of the  $sloscillations\_ISTA$  model spectra to apply the sigmoid profile from equation 4.1. From an  $sloscillations\_ISTA$  model, the power spectra comprising of the  $\ell=0,1,2,3$  modes as well as only the  $\ell=0,2,3$  modes can be extracted. With the two model spectra of the same star,  $PSD_{\ell=0,1,2,3}$  and  $PSD_{\ell=0,2,3}$ , an isolated power spectra density of  $\ell=1$  modes can be achieved from the difference of the two, following  $PSD_{\ell=1}=PSD_{\ell=0,2,3}-PSD_{0,1,2,3}$ . Equation 4.1 is then multiplied into  $PSD_{\ell=1}$  such that only high frequency mode amplitudes are visible. The resultant sigmoid altered spectra  $PSD_S$  is then added back to the spectra containing only  $\ell=0,2,3$ ,  $PSD_{\ell=0,2,3}$ , to yield the sigmoid altered model illustrated in figure 4.3.

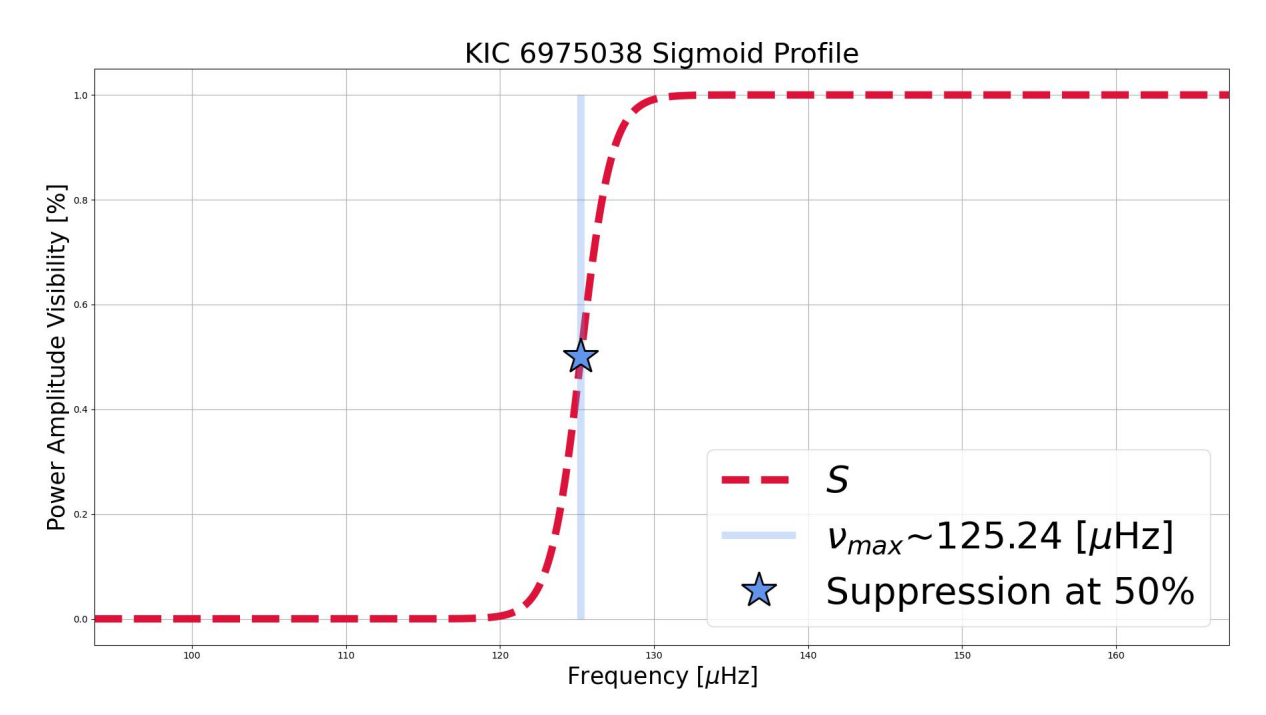


Figure 4.2: The Sigmoid function plotted with the red dashed line is created using equation 4.1 for the relevant frequency range of the partially suppressed star KIC 6975038. The vertical blue line shows  $\nu_{max}\approx 125.24~[\mu {\rm Hz}]$ , and the blue star shows the inflection or mid-point (50% mode suppression) of the Sigmoid function with a default setting at  $\nu_{max}$ . The Sigmoid function has a sharp change of behaviour from 0% to 100% to imitate the change from total suppression to the reappearance of the dipole  $\ell=1$  mixed mode; with this transition occurring near  $\nu_{max}$ , justifying the choice to set the inflection point at  $\nu_{max}$ .

#### 4.2.2 KIC 6975038: The Unusual Red Giant

In this section, we report on the results of the Bayesian fitting of the parameters of the *Kepler* red giant KIC 6975038. Table 4.2 displays the estimated parameter values for the star as well as the respective uncertainties, as calculated in *Bayessloscillations\_ISTA* (Desai et. al., in prep.).

The best fit model of the stellar power spectra for KIC 6975038 is seen in figure 4.3 which showcases a comparison of the original data, the sigmoid altered *sloscillations\_ISTA* prior model, and the resultant *Bayessloscillations\_ISTA* model with the sigmoid profile superimposed for visualization of the mode suppression; the  $\ell=0,2,3$  mode frequencies are also highlighted for easier identification of the dipole  $\ell=1$  modes that are present in the space between  $\ell=3$  and  $\ell=2$ . The best fit model parameters are listed in table 4.2. Of note for the characterization of a potential magnetic perturbation,  $\delta\nu_{mag}$  is a non-zero value, indicative of a magnetic modulation on the dipolar mixed modes.

The posterior distribution and chain of walkers from the Bayesian model fit are displayed in figures 4.4 and 4.5, respectively. From the model posterior distribution in figure 4.4 it can be seen that the parameters  $q, \delta\nu_{rot}, a, \epsilon_p, \Delta\nu$ , and  $\Delta\Pi_{\ell=1}$ , are well constrained parameters; noting that the distribution for  $\Delta\Pi_{\ell=1}$  appears to be pushing towards the boundary, as such, a case can be made that with adjusted boundaries this parameter may continue to move and is thus not well constrained. For the parameters  $\theta_{inc}, \epsilon_g$ , and  $\delta\nu_{mag}$ , the posterior distributions are more broad indicating that the parameters were more difficult to constrain.

Although the magnetic splitting determined by the Bayesian fitting of this work points towards

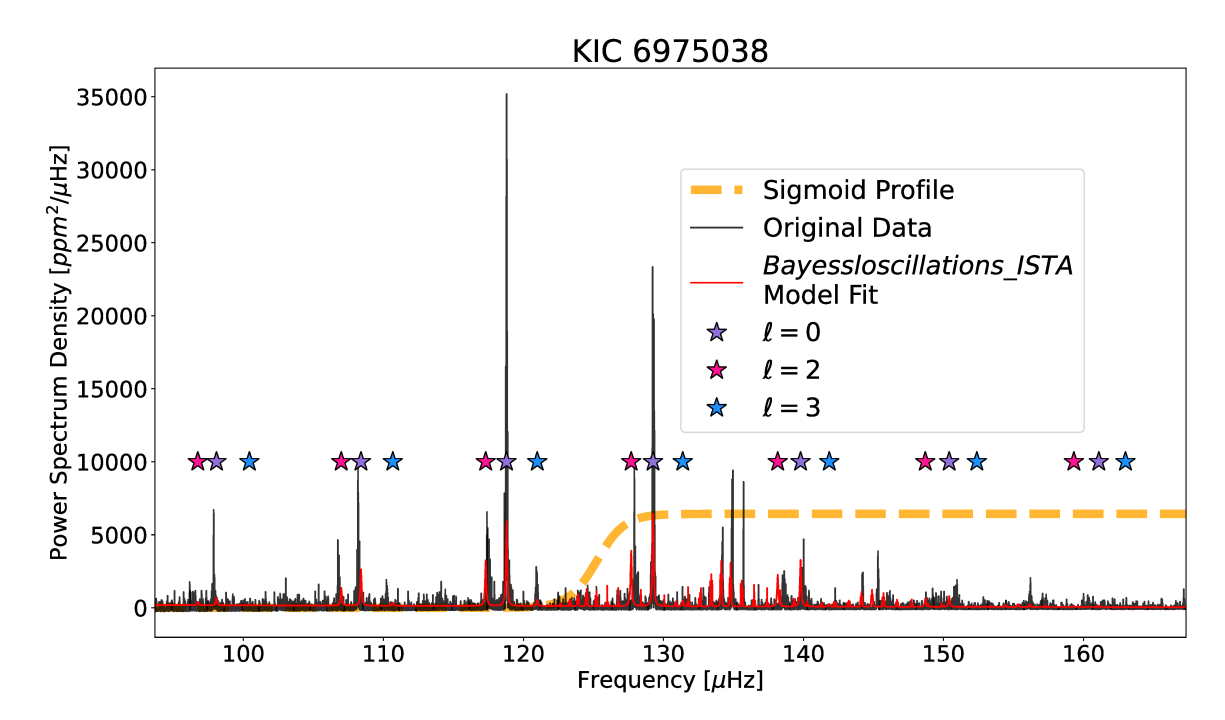


Figure 4.3: The resultant PSD of KIC 6975038 is shown in red plotted over the original data in black. In addition to what is shown in figure 4.1, the sigmoid profile used to modulate the dipolar component of the spectrum is illustrated by the orange dashed curve. For clarity in locating the  $\ell=1$  dipole mode regions, the  $\ell=0,2,3$  modes are highlighted with purple, pink, and blue stars respectively, such that the  $\ell=1$  oscillation modes reside between the  $\ell=2$  and  $\ell=3$  modes.

Fit Parameters			
Parameter	KIC 6975038		
$\Delta  u  [\mu {\sf Hz}]$	$10.474^{+0.005}_{-0.005}$		
$\delta  u_{mag} \ [\mu { m Hz}]$	$0.138^{+0.039}_{-0.049}$		
$\delta  u_{rot} \ [\mu  extsf{Hz}]$	$0.163^{+0.077}_{-0.064}$		
$\theta_{inc}$ [°]	$49.2_{-7}^{+6}$		
a [unitless]	$-0.019^{+0.120}_{-0.129}$		
q [unitless]	$0.207^{+0.017}_{-0.018}$		
$\epsilon_g$ [unitless]	$0.115^{+0.206}_{-0.234}$		
$\epsilon_p$ [unitless]	$0.340^{+0.006}_{-0.006}$		
$\Delta\Pi_{\ell=1}$ [seconds]	$51.090^{+1.630}_{-0.434}$		

Table 4.2: List of the fit model parameters from *Bayessloscillations\_ISTA* (Desai et al. in prep.) including the respective errors measured as the difference between the mean and 16th and 84th percentiles from the resultant MCMC chain of walkers.

the presence of an interior magnetic field, the  $\delta\nu_{mag}=0.138^{+0.039}_{-0.049}~[\mu {\rm Hz}]$  estimated in this study is outside of the margins of error for the  $\delta\nu_{mag}=7.18^{+0.03}_{-0.03}~[\mu {\rm Hz}]$  reported by [DLBL23]. Additionally, the parameters q and  $\Delta\Pi_{\ell=1}$  are again in disagreement with reported literature values, where [MBP+17, MPB+17] and [VMS16] report coupling values of  $q=0.35^{+0.03}_{-0.03}$  and q=0.17, respectively. And [MBP+17, MPB+17] and [VMS16] report period spacings of  $\Delta\Pi_{\ell=1}=57.9,~\Delta\Pi_{\ell=1}=74.1^{+5}_{-5}$  respectively, while [DLBL23] reports values of  $\Delta\Pi_{\ell=1}=63.5$  and  $\Delta\Pi_{\ell=1}=82.22^{+0.08}_{-0.08}$ . In [DLBL23], the period spacing is initially estimated using traditional

#### 4. Results

Figure 4.4: The posterior distribution of the <code>Bayessloscillations\_ISTA</code> (Desai et al. in prep.) fit for the power spectrum of KIC 6975038 is shown, illustrating that some of the parameters, namely  $\theta_{inc}, \epsilon_g$  and  $\delta\nu_{mag}$ , are not as well constrained as  $q, \Delta\nu$  or  $\epsilon_p$ . Of note is the distribution for  $\Delta\Pi_{\ell=1}$ , which is in agreement with red giant values ( $\sim 50 < \Delta\Pi_{\ell=1} < \sim 150$ ) according to [MBB+14], although the value is on the lower end of this boundary and so further evaluation of this behavior is needed.

estimation methods for this parameter which yields the first value that is noticeably smaller than stars within a similar  $\Delta\nu$  range; their second estimation of this parameter is computed by lining up the azimuthal components m of the dipole modes such that they are approximately evenly spaced in period (as it the expected case for pure g-modes, while pure p-modes are expected to be evenly spaced in frequency by  $\Delta\nu$ ). The two reported values from different in [DLBL23] highlights a note made in [MPB+17], being that the measures period spacing for stars with magnetic modulations, is significantly lower than that of the asymptotic period spacing for the same star. [MPB+17] notes both a low  $\Delta\Pi_{\ell=1}$  and a high q for KIC 6975038, noting that these unusual values for a star with  $\Delta\nu\approx 10.474^{+0.005}_{-0.005}$  [ $\mu$ Hz] may be indicative of a larger radiative cavity, resulting in a smaller region between the radiative interior and the convective envelope that allows for more p and g-mode coupling before the modes become evanescent and decay rather than coupling.

As mentioned previously with the inclination  $\theta_{inc}$ , this parameter is often used in studies at the start to restrict the sample to only include targets where all of the azimuthal components

of the oscillation modes are visible. Without a good constraint on the stellar inclination  $\theta_{inc}$  it is consistent that the magnetic and rotational parameters that depend on these components are also not well constrained; furthermore, without dedicated studies on the fundamental parameters of this particular target considering the unique profile, it will continue to be difficult to characterize the mixed mode pattern.

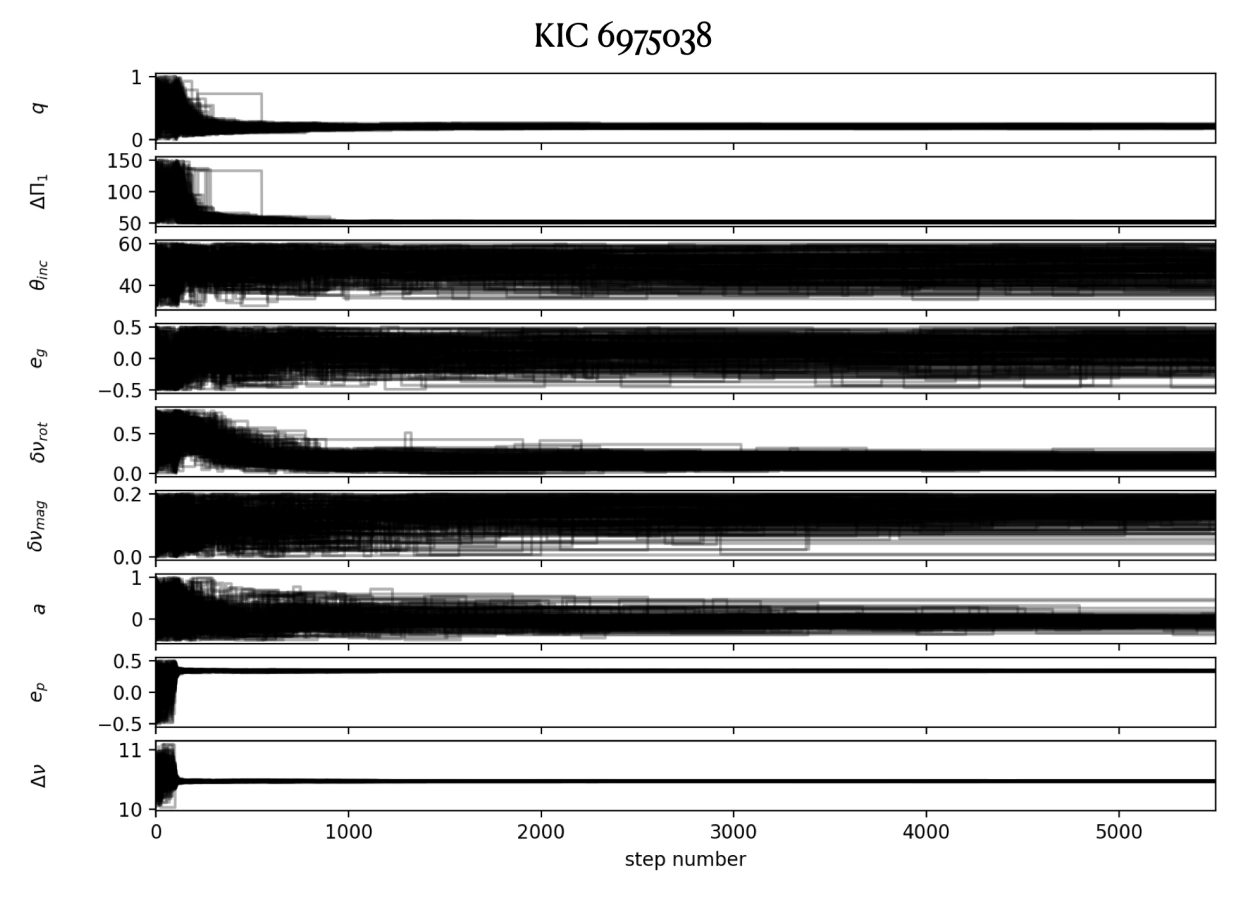


Figure 4.5: The MCMC walker chains of the *Bayessloscillations\_ISTA* (Desai et al. in prep.) fit for the power spectrum of KIC 6975038 is shown and illustrates the parameter exploration of the walkers.

## Discussion, Conclusions, & Interpretations

As the goal of this study was to investigate if the suppressed dipole mode amplitudes in red giant stars are exhibited simultaneously with the magnetic frequency shifts of the same modes, the magnetic shift,  $\delta\nu_{mag}$ , and asymmetry, a, parameters will help in answering this inquiry. The asymmetry a and magnetic shift  $\delta\nu_{maq}$  listed in table 4.2 would indicate towards there being an internal magnetic field inducing a perturbation of the dipole mixed mode oscillation frequencies, with the non-zero value of  $\delta \nu_{maq}$ . As [DLBL23] also report a non-zero magnetic shift for KIC 6975038 which also presents with partially suppressed dipole mixed modes, it can be said that both mode suppression and magnetic shifting of dipole mixed modes can occur simultaneously. Although, there are two caveats of note here, one being that multiple parameters reported in this study for KIC 6975038 (namely  $\delta\nu_{mag}, q$ , and  $\Delta\Pi_{\ell=1}$ ) are not within the margins of errors of the previously reported literature values (see [MBP+17, MPB+17], [VMS16], [DLBL23]), and the second being that KIC 6975038 is currently the only red giant star reported to present with both mode suppression and magnetic frequency shifts. To further validate the simultaneous existence of mode suppression and magnetic frequency shifts and determine how the two characteristics interact with one another with varying magnetic field strengths and topologies, a larger sample of these partially suppressed stars will need to be identified and characterized; a key takeaway from this work is the potential for target selection of partially suppressed red giants by means of the dipole mode visibilities discussed in section 2.4 wherein our initial guess is that stars with partially suppressed dipole mode amplitudes will have (near-)intermediate visibility measurements,  $V_{\ell=1}^2$ . Additionally, as it is noted in [MBP+17] and further elaborated on in [MPB+17], KIC 6975038 was investigated because of the star's unusually high coupling parameter, q, and later noted by both [MPB<sup>+</sup>17] and [DLBL23] for the unusually low  $\Delta\Pi_{\ell=1}$ ; as such, another search criteria for partially suppressed stars can be via unusual outliers in stellar parameters describing mixed modes.

The Bayesian model fit parameters of KIC 6975038 in table 4.2 show  $\delta\nu_{mag}$ , is non-zero and indicative of a magnetic signature in this star with the current models. From figure 4.3 the original data and the Bayesian fit model are a close match, with the model deviating slightly from the data across the spectrum. Notably, the  $\ell=0$  dipole mode frequencies appear to be estimated relatively well between  $130\mu{\rm Hz}$  and  $140~\mu{\rm Hz}$ , but the same cannot be said for the following radial order, n, at high frequency. With that, it is evident that the Bayessloscillations\_ISTA (Desai et al. in prep.) is performing moderately well in fitting the

PSD, including the complicated mixed mode pattern, but user-dependent adjustments still need to be made to achieve improvements in the fitting to create trustworthy models; these user dependent adjustments include better constraints on the stellar input parameters of the model that remain constant and are not fit in the Bayesian procedure, including but not limited to  $\nu_{max}$ ,  $\alpha_{\ell=1}$ ,  $T_{eff}$  (the effective temperature), and  $\delta_{01}$  as described in section 3.

We can conclude that the *Kepler* red giant KIC 6975038, with partially suppressed dipole oscillation modes, may contain magnetic signatures in the form of frequency shifts (as reported in [DLBL23]), but updated models and further evaluation of the individual oscillations modes may need to be conducted for a definitive conclusion with the modeling and Bayesian fitting methods of this work using *sloscillations\_ISTA* and *Bayessloscillations\_ISTA* (Desai et al. in prep.).

Furthermore, we plan extend this study to a larger sample of stars following the target selection from section 2.4, aiming towards painting a more clear picture of the frequency pattern in low amplitude mixed modes.

## **Bibliography**

- [ACK10] Conny Aerts, Jørgen Christensen-Dalsgaard, and Donald W. Kurtz. *Asteroseis-mology*. Springer Dordrecht, 2010.
- [AT24] C. Aerts and A. Tkachenko. Asteroseismic modelling of fast rotators and its opportunities for astrophysics. *A&A*, 692:1–38, January 2024.
- [BBB+14] O. Benomar, K. Belkacem, T. R. Bedding, D. Stello, M. P. Di Mauro, R. Ventura, B. Mosser, M. J. Goupil, R. Samadi, and R. A. Garcia. Asteroseismology of Evolved Stars with Kepler: A New Way to Constrain Stellar Interiors Using Mode Inertias., 781(2):L29, February 2014.
- [BBM+11] P. G. Beck, T. R. Bedding, B. Mosser, D. Stello, R. A. Garcia, T. Kallinger, S. Hekker, Y. Elsworth, S. Frandsen, F. Carrier, J. De Ridder, C. Aerts, T. R. White, D. Huber, M. A. Dupret, J. Montalbán, A. Miglio, A. Noels, W. J. Chaplin, H. Kjeldsen, J. Christensen-Dalsgaard, R. L. Gilliland, T. M. Brown, S. D. Kawaler, S. Mathur, and J. M. Jenkins. Kepler Detected Gravity-Mode Period Spacings in a Red Giant Star. Science, 332(6026):205, April 2011.
- [BDA+12] P. G. Beck, J. De Ridder, C. Aerts, T. Kallinger, S. Hekker, R. A. García, B. Mosser, and G. R. Davies. Constraining the core-rotation rate in red-giant stars from Kepler space photometry. Astronomische Nachrichten, 333(10):967, December 2012.
- [BDB<sup>+</sup>24] Shatanik Bhattacharya, Srijan Bharati Das, Lisa Bugnet, Subrata Panda, and Shravan M. Hanasoge. Detectability of Axisymmetric Magnetic Fields from the Core to the Surface of Oscillating Post-main-sequence Stars. *ApJ*, 970(1):42, July 2024.
- [BGB<sup>+</sup>22] S. N. Breton, R. A. Garc'ia, J. Ballot, V. Delsanti, and D. Salabert. Deciphering stellar chorus: apollinaire, a Python 3 module for Bayesian peakbagging in helioseismology and asteroseismology. *A&A*, 663:A118, July 2022.
- [BKB+10] William J. Borucki, David Koch, Gibor Basri, Natalie Batalha, Timothy Brown, Douglas Caldwell, John Caldwell, Jørgen Christensen-Dalsgaard, William D. Cochran, Edna DeVore, Edward W. Dunham, Andrea K. Dupree, Thomas N. Gautier, John C. Geary, Ronald Gilliland, Alan Gould, Steve B. Howell, Jon M. Jenkins, Yoji Kondo, David W. Latham, Geoffrey W. Marcy, Søren Meibom, Hans Kjeldsen, Jack J. Lissauer, David G. Monet, David Morrison, Dimitar Sasselov, Jill Tarter, Alan Boss, Don Brownlee, Toby Owen, Derek Buzasi, David Charbonneau, Laurance Doyle, Jonathan Fortney, Eric B. Ford, Matthew J. Holman, Sara Seager, Jason H. Steffen, William F. Welsh, Jason Rowe, Howard Anderson,

Lars Buchhave, David Ciardi, Lucianne Walkowicz, William Sherry, Elliott Horch, Howard Isaacson, Mark E. Everett, Debra Fischer, Guillermo Torres, John Asher Johnson, Michael Endl, Phillip MacQueen, Stephen T. Bryson, Jessie Dotson, Michael Haas, Jeffrey Kolodziejczak, Jeffrey Van Cleve, Hema Chandrasekaran, Joseph D. Twicken, Elisa V. Quintana, Bruce D. Clarke, Christopher Allen, Jie Li, Haley Wu, Peter Tenenbaum, Ekaterina Verner, Frederick Bruhweiler, Jason Barnes, and Andrej Prsa. Kepler Planet-Detection Mission: Introduction and First Results. *Science*, 327(5968):977, February 2010.

- [BMH+11] Timothy R. Bedding, Benoit Mosser, Daniel Huber, Josefina Montalbán, Paul Beck, Jørgen Christensen-Dalsgaard, Yvonne P. Elsworth, Rafael A. García, Andrea Miglio, Dennis Stello, Timothy R. White, Joris De Ridder, Saskia Hekker, Conny Aerts, Caroline Barban, Kevin Belkacem, Anne-Marie Broomhall, Timothy M. Brown, Derek L. Buzasi, Fabien Carrier, William J. Chaplin, Maria Pia di Mauro, Marc-Antoine Dupret, Søren Frandsen, Ronald L. Gilliland, Marie-Jo Goupil, Jon M. Jenkins, Thomas Kallinger, Steven Kawaler, Hans Kjeldsen, Savita Mathur, Arlette Noels, Victor Silva Aguirre, and Paolo Ventura. Gravity modes as a way to distinguish between hydrogen- and helium-burning red giant stars. *Nature*, 471(7340):608–611, March 2011.
- [BPB22] K. Belkacem, C. Pinçon, and G. Buldgen. Amplitudes of Solar Gravity Modes: A Review. *SoPh*, 297(11):147, November 2022.
- [BPM+21] L. Bugnet, V. Prat, S. Mathis, A. Astoul, K. Augustson, R. A. García, S. Mathur, L. Amard, and C. Neiner. Magnetic signatures on mixed-mode frequencies. I. An axisymmetric fossil field inside the core of red giants. A&A, 650:A53, June 2021.
- [Bug22] L. Bugnet. Magnetic signatures on mixed-mode frequencies. II. Period spacings as a probe of the internal magnetism of red giants., 667:A68, November 2022.
- [CDG15] E. Corsaro, J. De Ridder, and R. A. García. Bayesian peak bagging analysis of 19 low-mass low-luminosity red giants observed with Kepler. *A&A*, 579:A83, July 2015.
- [CFB16] Matteo Cantiello, Jim Fuller, and Lars Bildsten. Asteroseismic Signatures of Evolving Internal Stellar Magnetic Fields. *ApJ*, 824(1):14, June 2016.
- [Chr04] JØrgen Christensen-Dalsgaard. Physics of solar-like oscillations. *SoPh*, 220(2):137–168, April 2004.
- [CMB<sup>+</sup>14] Matteo Cantiello, Christopher Mankovich, Lars Bildsten, Jørgen Christensen-Dalsgaard, and Bill Paxton. Angular Momentum Transport within Evolved Low-mass Stars. *ApJ*, 788(1):93, June 2014.
- [CSH+12] Enrico Corsaro, Dennis Stello, Daniel Huber, Timothy R. Bedding, Alfio Bonanno, Karsten Brogaard, Thomas Kallinger, Othman Benomar, Timothy R. White, Benoit Mosser, Sarbani Basu, William J. Chaplin, Jørgen Christensen-Dalsgaard, Yvonne P. Elsworth, Rafael A. García, Saskia Hekker, Hans Kjeldsen, Savita Mathur, Søren Meibom, Jennifer R. Hall, Khadeejah A. Ibrahim, and Todd C. Klaus. Asteroseismology of the Open Clusters NGC 6791, NGC 6811, and NGC 6819 from 19 Months of Kepler Photometry. ApJ, 757(2):190, October 2012.

- [DBB<sup>+</sup>15] S. Deheuvels, J. Ballot, P. G. Beck, B. Mosser, R. Østensen, R. A. García, and M. J. Goupil. Seismic evidence for a weak radial differential rotation in intermediate-mass core helium burning stars. , 580:A96, August 2015.
- [DEB24] S. B. Das, L. Einramhof, and L. Bugnet. Unveiling complex magnetic field configurations in red giant stars. *A&A*, 690:A217, October 2024.
- [DFP95] V. Domingo, B. Fleck, and A. I. Poland. The SOHO Mission: an Overview. *SoPh*, 162(1-2):1–37, December 1995.
- [DGHS01] W. A. Dziembowski, D. O. Gough, G. Houdek, and R. Sienkiewicz. Oscillations of  $\alpha$  UMa and other red giants. *MNRAS*, 328(2):601–610, December 2001.
- [DLBL23] S. Deheuvels, G. Li, J. Ballot, and F. Lignières. Strong magnetic fields detected in the cores of 11 red giant stars using gravity-mode period spacings. *A&A*, 670:L16, February 2023.
- [EHI<sup>+</sup>94] Y. Elsworth, R. Howe, G. R. Isaak, C. P. McLeod, B. A. Miller, R. New, C. C. Speake, and S. J. Wheeler. Solar p-Mode Frequencies and Their Dependence on Solar Activity: Recent Results from the BISON Network. *ApJ*, 434:801, October 1994.
- [FAA<sup>+</sup>97] Claus Fröhlich, Bo N. Andersen, Thierry Appourchaux, Gabrielle Berthomieu, Dominique A. Crommelynck, Vicente Domingo, Alain Fichot, Wolfgang Finsterle, Maria F. Gómez, Douglas Gough, Antonio Jiménez, Torben Leifsen, Marc Lombaerts, Judit M. Pap, Janine Provost, Teodoro Roca Cortés, José Romero, Hansjörg Roth, Takashi Sekii, Udo Telljohann, Thierry Toutain, and Christoph Wehrli. First Results from VIRGO, the Experiment for Helioseismology and Solar Irradiance Monitoring on SOHO. SoPh, 170(1):1–25, January 1997.
- [FCS<sup>+</sup>15] Jim Fuller, Matteo Cantiello, Dennis Stello, Rafael A. Garcia, and Lars Bildsten. Asteroseismology can reveal strong internal magnetic fields in red giant stars. *Science*, 350(6259):423–426, October 2015.
- [FHLG13] Daniel Foreman-Mackey, David W. Hogg, Dustin Lang, and Jonathan Goodman. emcee: The MCMC Hammer. *PASP*, 125(925):306, March 2013.
- [FPJ19] Jim Fuller, Anthony L. Piro, and Adam S. Jermyn. Slowing the spins of stellar cores. *MNRAS*, 485(3):3661–3680, May 2019.
- [GAC+08] F. Grundahl, T. Arentoft, J. Christensen-Dalsgaard, S. Frandsen, H. Kjeldsen, and P. K. Rasmussen. Stellar Oscillations Network Group SONG. In *Journal of Physics Conference Series*, volume 118 of *Journal of Physics Conference Series*, page 012041. IOP, October 2008.
- [GGC<sup>+</sup>95] A. H. Gabriel, G. Grec, J. Charra, J. M. Robillot, T. Roca Cortés, S. Turck-Chièze, R. Bocchia, P. Boumier, M. Cantin, E. Cespédes, B. Cougrand, J. Crétolle, L. Damé, M. Decaudin, P. Delache, N. Denis, R. Duc, H. Dzitko, E. Fossat, J. J. Fourmond, R. A. García, D. Gough, C. Grivel, J. M. Herreros, H. Lagardère, J. P. Moalic, P. L. Pallé, N. Pétrou, M. Sanchez, R. Ulrich, and H. B. van der Raay. Global Oscillations at Low Frequency from the SOHO Mission (GOLF). SoPh, 162(1-2):61–99, December 1995.

- [GHS+11] R. A. García, S. Hekker, D. Stello, J. Gutiérrez-Soto, R. Handberg, D. Huber, C. Karoff, K. Uytterhoeven, T. Appourchaux, W. J. Chaplin, Y. Elsworth, S. Mathur, J. Ballot, J. Christensen-Dalsgaard, R. L. Gilliland, G. Houdek, J. M. Jenkins, H. Kjeldsen, S. McCauliff, T. Metcalfe, C. K. Middour, J. Molenda-Zakowicz, M. J. P. F. G. Monteiro, J. C. Smith, and M. J. Thompson. Preparation of Kepler light curves for asteroseismic analyses. MNRAS, 414(1):L6–L10, June 2011.
- [GL20] Pedro Gomes and Ilídio Lopes. Core magnetic field imprint in the non-radial oscillations of red giant stars. MNRAS, 496(1):620–628, July 2020.
- [GMM+13] M. J. Goupil, B. Mosser, J. P. Marques, R. M. Ouazzani, K. Belkacem, Y. Lebreton, and R. Samadi. Seismic diagnostics for transport of angular momentum in stars. II. Interpreting observed rotational splittings of slowly rotating red giant stars. A&A, 549:A75, January 2013.
- [GMM<sup>+</sup>18] C. Gehan, B. Mosser, E. Michel, R. Samadi, and T. Kallinger. Core rotation braking on the red giant branch for various mass ranges. *A&A*, 616:A24, August 2018.
- [GMMC21] C. Gehan, B. Mosser, E. Michel, and M. S. Cunha. Automated approach to measure stellar inclinations: validation through large-scale measurements on the red giant branch. A&A, 645:A124, January 2021.
- [GPB+14] R. A. García, F. Pérez Hernández, O. Benomar, V. Silva Aguirre, J. Ballot, G. R. Davies, G. Doğan, D. Stello, J. Christensen-Dalsgaard, G. Houdek, F. Lignières, S. Mathur, M. Takata, T. Ceillier, W. J. Chaplin, S. Mathis, B. Mosser, R. M. Ouazzani, M. H. Pinsonneault, D. R. Reese, C. Régulo, D. Salabert, M. J. Thompson, J. L. van Saders, C. Neiner, and J. De Ridder. Study of KIC 8561221 observed by Kepler: an early red giant showing depressed dipolar modes. A&A, 563:A84, March 2014.
- [Har85] J. Harvey. High-Resolution Helioseismology. In Erica Rolfe and Bruce Battrick, editors, Future Missions in Solar, Heliospheric & Space Plasma Physics, volume 235 of ESA Special Publication, page 199, June 1985.
- [HHH+96] J. W. Harvey, F. Hill, R. P. Hubbard, J. R. Kennedy, J. W. Leibacher, J. A. Pintar, P. A. Gilman, R. W. Noyes, A. M. Title, J. Toomre, R. K. Ulrich, A. Bhatnagar, J. A. Kennewell, W. Marquette, J. Patron, O. Saa, and E. Yasukawa. The Global Oscillation Network Group (GONG) Project. *Science*, 272(5266):1284–1286, May 1996.
- [HON+24] Emily J. Hatt, J. M. Joel Ong, Martin B. Nielsen, William J. Chaplin, Guy R. Davies, Sébastien Deheuvels, Jérôme Ballot, Gang Li, and Lisa Bugnet. Asteroseismic signatures of core magnetism and rotation in hundreds of low-luminosity red giants. *MNRAS*, 534(2):1060–1076, October 2024.
- [HSY17] Marc Hon, Dennis Stello, and Jie Yu. Deep learning classification in asteroseismology. *MNRAS*, 469(4):4578–4583, August 2017.
- [HSY18] Marc Hon, Dennis Stello, and Jie Yu. Deep learning classification in asteroseismology using an improved neural network: results on 15 000 Kepler red giants and applications to K2 and TESS data. MNRAS, 476(3):3233–3244, May 2018.

- [KCN+19] James S. Kuszlewicz, William J. Chaplin, Thomas S. H. North, Will M. Farr, Keaton J. Bell, Guy R. Davies, Tiago L. Campante, and Saskia Hekker. Bayesian hierarchical inference of asteroseismic inclination angles. , 488(1):572–589, September 2019.
- [KDH+14] T. Kallinger, J. De Ridder, S. Hekker, S. Mathur, B. Mosser, M. Gruberbauer, R. A. García, C. Karoff, and J. Ballot. The connection between stellar granulation and oscillation as seen by the Kepler mission. A&A, 570:A41, October 2014.
- [KHH23] James S. Kuszlewicz, Marc Hon, and Daniel Huber. Mixed-mode Ensemble Asteroseismology of Low-luminosity Kepler Red Giants. *ApJ*, 954(2):152, September 2023.
- [LDB24] Gang Li, Sébastien Deheuvels, and Jérôme Ballot. Asteroseismic measurement of core and envelope rotation rates for 2006 red giant branch stars. *A&A*, 688:A184, August 2024.
- [LDBL22] Gang Li, Sébastien Deheuvels, Jérôme Ballot, and François Lignières. Magnetic fields of 30 to 100 kG in the cores of red giant stars. *Nature*, 610(7930):43–46, October 2022.
- [LDL<sup>+</sup>23] Gang Li, Sébastien Deheuvels, Tanda Li, Jérôme Ballot, and François Lignières. Internal magnetic fields in 13 red giants detected by asteroseismology. *A&A*, 680:A26, December 2023.
- [Loi20] Shyeh Tjing Loi. Magneto-gravity wave packet dynamics in strongly magnetized cores of evolved stars. *MNRAS*, 493(4):5726–5742, April 2020.
- [Loi21] Shyeh Tjing Loi. Topology and obliquity of core magnetic fields in shaping seismic properties of slowly rotating evolved stars. *MNRAS*, 504(3):3711–3729, July 2021.
- [Lom76] N. R. Lomb. Least-Squares Frequency Analysis of Unequally Spaced Data. *ApSS*, 39(2):447–462, February 1976.
- [MB23] S. Mathis and L. Bugnet. Asymmetries of frequency splittings of dipolar mixed modes: A window on the topology of deep magnetic fields. *A&A*, 676:L9, August 2023.
- [MBA+06] E. Michel, A. Baglin, M. Auvergne, C. Catala, C. Aerts, G. Alecian, P. Amado, T. Appourchaux, M. Ausseloos, J. Ballot, C. Barban, F. Baudin, G. Berthomieu, P. Boumier, T. Bohm, M. Briquet, S. Charpinet, M. S. Cunha, P. De Cat, M. A. Dupret, J. Fabregat, M. Floquet, Y. Fremat, R. Garrido, R. A. Garcia, M. J. Goupil, G. Handler, A. M. Hubert, E. Janot-Pacheco, P. Lambert, Y. Lebreton, F. Lignieres, J. Lochard, S. Martin-Ruiz, P. Mathias, A. Mazumdar, P. Mittermayer, J. Montalban, M. J. P. F. G. Monteiro, P. Morel, B. Mosser, A. Moya, C. Neiner, P. Nghiem, A. Noels, J. Oehlinger, E. Poretti, J. Provost, J. Renan de Medeiros, J. De Ridder, M. Rieutord, T. Roca-Cortes, I. Roxburgh, R. Samadi, R. Scuflaire, J. C. Suarez, S. Theado, A. Thoul, T. Toutain, S. Turck-Chieze, K. Uytterhoeven, G. Vauclair, S. Vauclair, W. W. Weiss, and K. Zwintz. The Seismology Programme of CoRoT. In M. Fridlund, A. Baglin, J. Lochard, and L. Conroy, editors, The CoRoT Mission Pre-Launch Status Stellar Seismology

- and Planet Finding, volume 1306 of ESA Special Publication, page 39, November 2006.
- [MBA+08] Eric Michel, Annie Baglin, Michel Auvergne, Claude Catala, Reza Samadi, Frédéric Baudin, Thierry Appourchaux, Caroline Barban, Werner W. Weiss, Gabrielle Berthomieu, Patrick Boumier, Marc-Antoine Dupret, Rafael A. Garcia, Malcolm Fridlund, Rafael Garrido, Marie-Jo Goupil, Hans Kjeldsen, Yveline Lebreton, Benoît Mosser, Arlette Grotsch-Noels, Eduardo Janot-Pacheco, Janine Provost, Ian W. Roxburgh, Anne Thoul, Thierry Toutain, Didier Tiphène, Sylvaine Turck-Chieze, Sylvie D. Vauclair, Gérard P. Vauclair, Conny Aerts, Georges Alecian, Jérôme Ballot, Stéphane Charpinet, Anne-Marie Hubert, François Lignières, Philippe Mathias, Mario J. P. F. G. Monteiro, Coralie Neiner, Ennio Poretti, José Renan de Medeiros, Ignasi Ribas, Michel L. Rieutord, Teodoro Roca Cortés, and Konstanze Zwintz. CoRoT Measures Solar-Like Oscillations and Granulation in Stars Hotter Than the Sun. Science, 322(5901):558, October 2008.
- [MBB+14] B. Mosser, O. Benomar, K. Belkacem, M. J. Goupil, N. Lagarde, E. Michel, Y. Lebreton, D. Stello, M. Vrard, C. Barban, T. R. Bedding, S. Deheuvels, W. J. Chaplin, J. De Ridder, Y. Elsworth, J. Montalban, A. Noels, R. M. Ouazzani, R. Samadi, T. R. White, and H. Kjeldsen. Mixed modes in red giants: a window on stellar evolution. A&A, 572:L5, December 2014.
- [MBG+11] B. Mosser, K. Belkacem, M. J. Goupil, E. Michel, Y. Elsworth, C. Barban, T. Kallinger, S. Hekker, J. De Ridder, R. Samadi, F. Baudin, F. J. G. Pinheiro, M. Auvergne, A. Baglin, and C. Catala. The universal red-giant oscillation pattern. An automated determination with CoRoT data. A&A, 525:L9, January 2011.
- [MBP+17] B. Mosser, K. Belkacem, C. Pinçon, M. Takata, M. Vrard, C. Barban, M. J. Goupil, T. Kallinger, and R. Samadi. Dipole modes with depressed amplitudes in red giants are mixed modes. A&A, 598:A62, February 2017.
- [MBP+21] S. Mathis, L. Bugnet, V. Prat, K. Augustson, S. Mathur, and R. A. Garcia. Probing the internal magnetism of stars using asymptotic magneto-asteroseismology. *A&A*, 647:A122, March 2021.
- [MEH+12] B. Mosser, Y. Elsworth, S. Hekker, D. Huber, T. Kallinger, S. Mathur, K. Belkacem, M. J. Goupil, R. Samadi, C. Barban, T. R. Bedding, W. J. Chaplin, R. A. García, D. Stello, J. De Ridder, C. K. Middour, R. L. Morris, and E. V. Quintana. Characterization of the power excess of solar-like oscillations in red giants with Kepler. A&A, 537:A30, January 2012.
- [MGB+12a] B. Mosser, M. J. Goupil, K. Belkacem, J. P. Marques, P. G. Beck, S. Bloemen, J. De Ridder, C. Barban, S. Deheuvels, Y. Elsworth, S. Hekker, T. Kallinger, R. M. Ouazzani, M. Pinsonneault, R. Samadi, D. Stello, R. A. García, T. C. Klaus, J. Li, S. Mathur, and R. L. Morris. Spin down of the core rotation in red giants. A&A, 548:A10, December 2012.
- [MGB+12b] B. Mosser, M. J. Goupil, K. Belkacem, E. Michel, D. Stello, J. P. Marques, Y. Elsworth, C. Barban, P. G. Beck, T. R. Bedding, J. De Ridder, R. A. García, S. Hekker, T. Kallinger, R. Samadi, M. C. Stumpe, T. Barclay, and C. J. Burke. Probing the core structure and evolution of red giants using gravity-dominated mixed modes observed with Kepler. A&A, 540:A143, April 2012.

- [MGB<sup>+</sup>18] B. Mosser, C. Gehan, K. Belkacem, R. Samadi, E. Michel, and M. J. Goupil. Period spacings in red giants. IV. Toward a complete description of the mixed-mode pattern. A&A, 618:A109, October 2018.
- [MGR+10] S. Mathur, R. A. García, C. Régulo, O. L. Creevey, J. Ballot, D. Salabert, T. Arentoft, P. O. Quirion, W. J. Chaplin, and H. Kjeldsen. Determining global parameters of the oscillations of solar-like stars. A&A, 511:A46, February 2010.
- [MMB<sup>+</sup>13] B. Mosser, E. Michel, K. Belkacem, M. J. Goupil, A. Baglin, C. Barban, J. Provost, R. Samadi, M. Auvergne, and C. Catala. Asymptotic and measured large frequency separations. *A&A*, 550:A126, February 2013.
- [MPB<sup>+</sup>17] B. Mosser, C. Pinçon, K. Belkacem, M. Takata, and M. Vrard. Period spacings in red giants. III. Coupling factors of mixed modes. *A&A*, 600:A1, April 2017.
- [MVB<sup>+</sup>15] B. Mosser, M. Vrard, K. Belkacem, S. Deheuvels, and M. J. Goupil. Period spacings in red giants. I. Disentangling rotation and revealing core structure discontinuities. *A&A*, 584:A50, December 2015.
- [ROM23] Nicholas Z Rui, J M Joel Ong, and Stéphane Mathis. Asteroseismic g-mode period spacings in strongly magnetic rotating stars. MNRAS, 527(3):6346–6362, 11 2023.
- [RWV<sup>+</sup>14] George R. Ricker, Joshua N. Winn, Roland Vanderspek, David W. Latham, Gáspár. Á. Bakos, Jacob L. Bean, Zachory K. Berta-Thompson, Timothy M. Brown, Lars Buchhave, Nathaniel R. Butler, R. Paul Butler, William J. Chaplin, David Charbonneau, Jørgen Christensen-Dalsgaard, Mark Clampin, Drake Deming, John Doty, Nathan De Lee, Courtney Dressing, E. W. Dunham, Michael Endl, Francois Fressin, Jian Ge, Thomas Henning, Matthew J. Holman, Andrew W. Howard, Shigeru Ida, Jon Jenkins, Garrett Jernigan, John A. Johnson, Lisa Kaltenegger, Nobuyuki Kawai, Hans Kjeldsen, Gregory Laughlin, Alan M. Levine, Douglas Lin, Jack J. Lissauer, Phillip MacQueen, Geoffrey Marcy, P. R. McCullough, Timothy D. Morton, Norio Narita, Martin Paegert, Enric Palle, Francesco Pepe, Joshua Pepper, Andreas Quirrenbach, S. A. Rinehart, Dimitar Sasselov, Bun'ei Sato, Sara Seager, Alessandro Sozzetti, Keivan G. Stassun, Peter Sullivan, Andrew Szentgyorgyi, Guillermo Torres, Stephane Udry, and Joel Villasenor. Transiting Exoplanet Survey Satellite (TESS). In Jacobus M. Oschmann, Jr., Mark Clampin, Giovanni G. Fazio, and Howard A. MacEwen, editors, Space Telescopes and Instrumentation 2014: Optical, Infrared, and Millimeter Wave, volume 9143 of Society of Photo-Optical Instrumentation Engineers (SPIE) Conference Series, page 914320, August 2014.
- [Sca82] J. D. Scargle. Studies in astronomical time series analysis. II. Statistical aspects of spectral analysis of unevenly spaced data. *ApJ*, 263:835–853, December 1982.
- [SCF+16a] Dennis Stello, Matteo Cantiello, Jim Fuller, Rafael A. Garcia, and Daniel Huber. Suppression of Quadrupole and Octupole Modes in Red Giants Observed by Kepler \*. *PASA*, 33:e011, March 2016.
- [SCF+16b] Dennis Stello, Matteo Cantiello, Jim Fuller, Daniel Huber, Rafael A. García, Timothy R. Bedding, Lars Bildsten, and Victor Silva Aguirre. A prevalence of dynamo-generated magnetic fields in the cores of intermediate-mass stars. *Nature*, 529(7586):364–367, January 2016.

- [Shi79] H. Shibahashi. Modal Analysis of Stellar Nonradial Oscillations by an Asymptotic Method., 31:87–104, January 1979.
- [SP00] Alison Sills and M. H. Pinsonneault. Rotation of Horizontal-Branch Stars in Globular Clusters. *ApJ*, 540(1):489–503, September 2000.
- [Tas80] M. Tassoul. Asymptotic approximations for stellar nonradial pulsations. , 43:469–490, August 1980.
- [UOA+89] Wasaburo Unno, Yoji Osaki, Hiroyasu Ando, H. Saio, and H. Shibahashi. *Nonradial oscillations of stars.* Tokyo: University of Tokyo Press, 1989.
- [VMS16] M. Vrard, B. Mosser, and R. Samadi. Period spacings in red giants. II. Automated measurement. *A&A*, 588:A87, April 2016.
- [YHB<sup>+</sup>18] Jie Yu, Daniel Huber, Timothy R. Bedding, Dennis Stello, Marc Hon, Simon J. Murphy, and Shourya Khanna. Asteroseismology of 16,000 Kepler Red Giants: Global Oscillation Parameters, Masses, and Radii. *ApJS*, 236(2):42, June 2018.